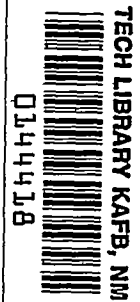


NACA RM L52I29

7370



NACA

RESEARCH MEMORANDUM

TOTAL-PRESSURE AND SCHLIEREN STUDIES OF THE WAKES OF
VARIOUS CANARD CONTROL SURFACES MOUNTED ON A
MISSILE BODY AT A MACH NUMBER OF 1.93

By William B. Boatright

Langley Aeronautical Laboratory
Langley Field, Va.

CLASSIFIED BY [REDACTED]
DATE [REDACTED]
OR [REDACTED]
MAINTAINED TO UNAUTHORIZED PERSON IS PROHIBITED BY LAW.

**NATIONAL ADVISORY COMMITTEE
FOR AERONAUTICS**

WASHINGTON

November 20, 1952

CLASSIFIED INFORMATION (OR TO BE DECLASSIFIED) *Unclassified*

BY *NASA Tech Rep Announcement #120*
(OFFICIAL USE ONLY) (DO NOT)

By

3 Oct 61

GRADE (OR TO BE DECLASSIFIED) *CHANGED*

30 Mar 61
DATE

AK



NATIONAL ADVISORY COMMITTEE FOR AERONAUTICS

RESEARCH MEMORANDUM

TOTAL-PRESSURE AND SCHLIEREN STUDIES OF THE WAKES OF
VARIOUS CANARD CONTROL SURFACES MOUNTED ON A
MISSILE BODY AT A MACH NUMBER OF 1.93

By William B. Boatright

SUMMARY

Wind-tunnel studies of the wake behind various canard control surfaces of equal span mounted on a missile body have been made at a Mach number of 1.93. The control-surface deflection was fixed at 9° and the range of angle of attack of the missile was from 0° to 3.5° . These studies were made for eight constant-span control surfaces of varying plan form, thickness, and section by means of total-pressure surveys at a location corresponding to a rearward ram-jet-engine inlet location and by means of schlieren photographs of the path of the rolled-up vortex sheet from the canard control surfaces. The effect of simulated, external rocket boosters on the pressure field was determined for three control-surface plan forms. In addition, the effect of end plates attached to the tips of one of the control surfaces was investigated.

The investigation revealed that reversed delta and delta control-surface plan forms gave locations of the core of the rolled-up vortex sheet from the canard control surfaces farther inboard than plan forms with straight tips. The core of the rolled-up vortex sheet was close to a location that was directly behind the tips in the free-stream direction for the straight-tipped plan forms, and was only slightly changed by angle of attack or Reynolds number for the range tested. Varying the control-surface thickness and profile also had very little effect on the pressure field at the survey plane. The effect of simulated rocket boosters on the body was to disperse the vortex cores over a greater region and to shift them outboard. Attaching end plates to a straight-trailing-edge plan form of 0.5 taper ratio produced an outboard shift of the vortex core from the tips and did not reduce the vortex strength enough to merit the use of end plates. Raking the tips of a control surface of this plan form produced only a slight inboard shift of the vortex core.

INTRODUCTION

A problem in the design of a ram-jet missile configuration is the selection of such relative locations of the engine inlet, the body, and the control surfaces that the interference effects from the body and control surfaces do not seriously impair the engine efficiency. At the same time the external drag should be kept at a minimum.

Analysis of the experimental data pertinent to this problem discloses the following trends: The data of reference 1 indicate losses in engine performance for a canard missile configuration employing normal-shock side inlets as the control surface deflection was varied. The maximum losses due to the vortex sheet shed from the canard control surface occurred for a missile angle of attack of 0° . The data of reference 2 indicate that, for a nacelle-mounted engine, severe losses in engine performance are encountered when the engine inlet is located directly behind the tips of the canard control surface; however, shifting the inlet outboard of these tips greatly improves the performance. In reference 3, force tests show that, from the standpoint of minimum external drag, the optimum engine location for the nacelle-mounted engine is the most inboard location tested. These opposing trends make the selection of the optimum ram-jet missile configuration difficult. References 4 and 5 present studies similar to the present investigation. The flow field at a rearward fuselage station is completely defined in these references by both total-pressure and flow-angle measurements for two different canard control surfaces. One control surface used was a triangular plan form and the other a 0.5-straight-taper plan form. In the present investigation more canard control-surface configurations were tested in the Langley 9-inch supersonic tunnel, but the measurements were limited to total-pressure surveys and schlieren studies.

The primary purpose of this investigation was to study the effects of some of the shape variables of the canard control surface, including plan form, thickness, and section, on the location of the shed vortex sheet. It was desired to find a configuration having reasonable lift effectiveness together with the most inboard location of the rolled-up vortex sheet. Such a configuration would allow the engine inlet to be mounted farther inboard for lower external drag, yet remain outboard of the rolled-up vortex sheet, so that better engine performance might be realized.

Throughout the present investigation the span of the canard control surfaces was constant and the locations of the rolled-up vortex sheet can be compared directly, although it should be remembered that, for some of the plan forms of lesser area or lift coefficient, higher deflection angles would be necessary to produce the same control. In addition to varying the plan form, thickness, and section of the canard surface, one of the canards was tested with end plates. Also, three of the plan forms were

CONFIDENTIAL

tested with simulated rocket boosters on the body. The total-pressure survey at a rearward station corresponding to the assumed engine inlet location and the plan-view schlieren photographs were taken for each configuration at missile angles of attack of 0° , 2° , and 3.5° .

SYMBOLS

H_3	total pressure behind normal shock as measured by tube aligned with free stream, in. Hg
H_0	tunnel stagnation pressure as measured in settling chamber of tunnel, in. Hg
H_2	total pressure behind a normal shock in the test section when free-stream Mach number is assumed, in. Hg
M	free-stream Mach number
R	Reynolds number
b	span, in.
x	axis in free-stream direction, in.
y	axis perpendicular to free stream and in spanwise direction of canard control surface, with origin at body center line, in.
z	axis perpendicular to both free stream and span of control surface with origin at juncture of control-surface trailing edge and body, in.
α	angle of attack, deg
δ	control-surface deflection referenced to body center line, deg
λ	taper ratio (ratio of tip chord to chord at juncture of control surface and body)

APPARATUS AND TESTS

Tunnel

The tests were made in the Langley 9-inch supersonic tunnel which is a continuously operating, closed-circuit type of tunnel in which the temperature, pressure, and humidity can be controlled. The test Mach

number is varied by interchangeable nozzles which form a test section about 9 inches square.

Model, Model Support, and Survey Apparatus

A photograph of the tunnel test section with the model and pitot tubes installed is shown in figure 1. Details of model construction are shown in figure 2. The body used in the present investigation is described in reference 6, and the various control surfaces tested are illustrated in figure 3. The canard control-surface deflection was constant at 9° . The plane of the angle of attack was horizontal and the apparatus for changing the angle of attack could be set at values of 0° , 2° , and 3.5° with the pivot point at the survey station. An optical system, consisting of a small mirror imbedded in the body at the pivot point and a circular screen located outside the test section upon which the light image reflected, was used to measure the angle of attack of the missile.

The total-pressure measurements were made with two rows of pitot tubes (0.040-inch outside diameter and 0.010-inch wall thickness). The rows were $\frac{3}{4}$ inch apart and the twelve tubes within each row were $\frac{3}{16}$ inch apart. These tubes could be traversed in both the y and z directions in the wake of a control surface with the tunnel operating. The rake of tubes was mounted on a tubular strut (2-inch outside diameter and 0.050-inch wall thickness) aligned with the stream. The pitot tubes remained parallel to the free stream throughout all testing. A cathetometer was used to measure the y location of the tubes and the z location was determined by a calibrated counter on the traversing lead screw.

Test Conditions

The tests were made at a Mach number of 1.93 and a tunnel stagnation pressure of approximately 114 inches of mercury. Additional surveys were made for some configurations at a stagnation pressure of approximately 31 inches of mercury to determine whether there were any noticeable Reynolds number effects over the possible range. These stagnation pressures produced Reynolds numbers of 1.13×10^6 and 0.31×10^6 per inch, respectively.

The humidity in the tunnel was kept sufficiently low so that any effects due to condensation were negligible.

Test Procedure

The total-pressure survey was made for each configuration and each angle of attack by setting the two rows of tubes at a given y value, then varying the location of the tubes in the z direction until they registered the point of minimum pressure. After the pressures were recorded for this condition, the z location was varied by about one-half the distance between the tubes ($\frac{3}{32}$ inch), maintaining the same y location to better define the wake profile. In some cases, three z locations for a given y were necessary where complicated profiles such as double peaks were encountered. The y locations were selected to permit wake profiles to be obtained across the core of the rolled-up vortex sheet and at stations inboard and outboard of this core. The schlieren apparatus was used in setting the y location of the tubes in order to observe the relative location of the tubes and the core of the rolled-up vortex sheet.

For some configurations an auxiliary shock phenomenon occurred when the low-energy air of the core of the vortex sheet passed midway between the two rows of tubes. This occurrence was a result of the separation of the low-energy air in the core when sufficient pressure from the shock system of the rake bled forward along the core. Since the phenomenon was obvious in the schlieren view screen, the y location could be selected to avoid invalidating the pressure readings for the configurations where it occurred. An example of such a phenomenon is illustrated in some of the schlieren photographs of figure 4 (for example, fig. 4(a)).

PRECISION OF DATA

The pitot tubes were aligned with the free stream throughout the tests and, consequently, in regions where the local flow angle was high, the measurements contain an error because of misalignment. The maximum flow angle reported in references 4 and 5 for similar configurations, however, was only about 8° , even near the center of the vortex core, and, as can be seen from the data of reference 7, any error due to this small amount of stream angle is negligible.

The estimated errors in the test parameters are as follows:

H_3/H_0 (higher R values)	±0.001
H_3/H_0 (lower R values)	±.002
y , in.	±.005
z , in.	±.015
α , deg	±.10
δ , deg	±.05

CONFIDENTIAL

RESULTS AND DISCUSSION

Schlieren Photographs

The paths of the vortex cores downstream from the canard control surfaces are illustrated in the schlieren photographs of figure 4. (All photographs were taken with the knife edge horizontal.) It can be seen that the presence of the expanding body downstream of the control surface causes an outboard shift in the paths of the vortex cores and that similarly the cores move in again as the body converges. Because of the small angle-of-attack range of the tests, very little effect due to angle of attack was discernible in the plan-view schlieren photographs. For this reason only two angles of attack are shown for each configuration (0° and 3.5°).

From figures 4(a), 4(b), and 4(c) it is evident that the control-surface thickness and section have little effect on the spanwise location of the vortex cores for the straight-trailing-edge plan form of taper ratio 0.5. At the survey station the cores appear almost directly behind the tips for each section and thickness variation. Similarly, in figures 4(d) and 4(e) the 0.697-taper plan form shows little difference due to thickness.

The schlieren photographs for the point-forward delta wing are shown in figure 4(f) and the reversed delta plan form in figure 4(g). Enlarged versions of the schlieren photographs clearly illustrated that the reversed delta plan form had the most inboard location of the vortex cores of all configurations tested. Based on the value of $b/2$ measured from the body center line at the survey station, the core for the reversed delta plan form was located from about $0.85b/2$ to $0.87b/2$ for all values of α tested. The next most inboard location was obtained with the point-forward delta plan form. For this plan form the vortex cores were located from about $0.88b/2$ to $0.94b/2$ for the same α range. In addition to being located farther inboard, the less distinct cores of the plan forms 3A and 2A (figs. 4(f) and 4(g)) indicate the density gradient across a core to be less abrupt. This result would indicate that these pointed-tip plan forms have either a weaker core or a more dispersed core. The pressure surveys to be discussed in the next section will show that a weaker core actually exists behind these pointed-tip plan forms and they, therefore, appear advantageous. The fact that the pointed-tip control surfaces are of smaller area and produce less lift tends to nullify this conclusion; however, if the control-surface deflection were increased to produce the same lift as the straight-tipped plan forms, only the strength of the core would be increased and the more inboard location of the core would still be realized. Conversely, if the control-surface area were increased to obtain the same lift, the location of the core would be shifted outboard but the weaker core would still be realized.

The effect of modifying plan form 1A by raking the tips 30° (fig. 4(h)) was only slightly favorable. This modification shifted the vortex cores from about $1.00b/2$ to $1.04b/2$ for the unmodified canard to about $0.97b/2$ to $1.00b/2$ for the control surface with raked tips.

Plan form 1A was also tested with end plates attached to the tips. The hypothesis was that the end plates would divide each vortex core behind the tips into two cores of less strength and thereby a favorable engine inlet location might be found. Figure 4(i) indicates that this modification divides the vortex core into two cores but the more outboard core appears much stronger than the inner core. Since the more outboard core is farther outboard than the core of a control surface with no end plates attached, the modification appears unfavorable with regard to the assumed inlet location. The pressure surveys (presented subsequently) confirm this conclusion since they also illustrate the z location and the strength of the core.

Plan forms 1D, 4C, and 2B were tested with simulated rocket boosters on the model, and the schlieren photographs of figures 4(j), 4(k), and 4(l) illustrate the flow patterns for these configurations. The effect of the boosters is to shift the vortex cores outboard considerably. For plan form 1D, which is plan form 1A with booster, the new location of the vortex cores is about $1.35b/2$ to $1.37b/2$ as compared with the location from about $1.00b/2$ to $1.04b/2$ without boosters. In addition, it can be seen that the boosters on the body cause a maze of shock and expansion waves in the region of the assumed inlet.

Pressure Surveys

Sample plots of the pressures as measured are illustrated in figures 5 to 9. The value of the pressure ratio at the peak is not shown in all cases since sometimes it was out of range of the manometer camera. From plots of this type it was possible to construct contour plots such as are presented in figures 10 to 21. The black dots in these figures are the points cross-plotted from the wake profiles used in the construction of the pressure contours and are shown in order that their accuracy in any particular region may be better assessed. The pressure ratio H_3/H_0 is the ratio of the total pressure behind a normal shock as measured by the pitot tube to the stagnation pressure as measured in the settling chamber of the tunnel. The values are not corrected for the loss through the normal shock generated by each tube since the local static pressure or Mach number was not measured; consequently, the values are not the true total-pressure recovery. In order to estimate the correlation between the values of H_3/H_0 which are presented (i.e., the measured values as obtained from a pitot tube) and the values of true total pressure recovery that would exist if a measuring instrument had no shock in front of it, the following arbitrary values are quoted:

Measured value	Corrected value
H_3/H_0	H_3/H_2
0.72	0.955
.70	.929
.68	.903

These arbitrary values, which are encountered near the assumed inlet, are based on the rough assumption that the Mach number of the flow is that of the free stream. The local Mach number of the flow may be subject to considerable variation from that of the free stream so these values should only be used in the crudest type of correlation. If the Mach number were 0.1 lower, the values would be off about 5.7 percent and, if the Mach number were 0.1 higher, the values would be off about 6.6 percent for the same values of H_3/H_0 . Although the data allow only rough estimates of the true total-pressure recovery by correcting the values in the foregoing manner, valid comparisons can be made among the various canard control surfaces as to their relative effects on the pressure field for the configurations tested.

In general, throughout all the configurations tested it can be seen that the effect of angle of attack for the small range investigated is very slight. The spanwise change in the location of the vortex cores is negligible, and there is a slight translation in the plus α direction. The latter result probably results from body upwash.

The effect of Reynolds number within the range tested is very slight. Figures 10 to 16 ((c) and (d) of each figure) show the only effect to be a slightly different z location of the vortex core. It is believed that this slight change in the z location is real, although it is close to the experimental accuracy.

A comparison of figures 10, 11, and 12 illustrates the effects of section profile and thickness on the pressure field behind a control surface of plan form 1. No outstanding effects appear and the y and z locations for the vortex core are almost identical in the three cases.

Contour plots for the reversed delta and point-forward delta plan forms are shown in figures 13 and 14. Both of these plan forms have pointed tips and, as suggested by the schlieren photographs, the vortex core is weaker than for the straight-tipped plan forms (i.e., the lowest values of H_3/H_0 in the vortex cores are of the order of 0.60 instead of 0.20 as is the case with the straight-tipped plan forms). Also, further corroborating the indications of the schlieren photographs, the vortex core for the reversed delta plan form is farthest inboard of all

the plan forms tested and only slightly farther outboard for the point-forward delta. From the schlieren photographs alone, the conclusion might be drawn that the vortex core is more dispersed and, consequently, the engine inlet not necessarily in a better pressure field. The contour plots clearly indicate, however, that the vortex cores are weaker and that the inlet could be moved farther inboard than for the other configurations before its lip encountered a lower pressure region. There also seems to be a tendency for the vortex sheet to roll up into more than one core; this tendency often occurs for plan forms of this type because the vorticity is more uniformly distributed across the span than for the straight-tipped plan forms. The apparent advantages of these pointed-tip plan forms must be somewhat nullified when the fact is considered that they are of smaller area and produce less lift than the other plan forms. A higher deflection, however, would only increase the strength of the cores and have little change on their spanwise location; whereas, a control surface of larger area would allow about an 18 percent increase in span for the same location of the rolled up vortex sheet, and the core would be weaker. The z location of the vortex cores for the delta and reversed delta is very nearly the same as for the other straight-tipped plan forms. Actually, the vortex cores near the tip appear to be slightly more in the plus α direction when the axis is considered to originate at the juncture of the trailing-edge root chord and the body.

The lack of any appreciable effect of thickness on plan form 4 can be seen by comparing figures 15 and 16. The vortex core is almost directly behind the tips for both cases and the pressure fields are very similar.

The pressure field for plan form 1F, which is plan form 1A with the tips raked 30° , is shown in figure 17. As the schlieren photographs showed, the vortex core is slightly more inboard for plan form 1F than for plan form 1A; but when considering whether the inlet could be moved farther inboard before experiencing unfavorable pressures, the 30° raked-tip wing is probably less satisfactory.

The unfavorable outboard shift of the vortex core due to the end plates is illustrated in figure 18. Although the core appears slightly weaker in strength, it is not weak enough to make the use of end plates favorable for a nacelle-mounted engine.

The unfavorable effect of the boosters is clearly indicated for the 0.5-taper, straight-trailing-edge plan form, 0.697-taper plan form, and reversed delta plan form in figures 19, 20, and 21. In general, the effect of the boosters is to disperse the low pressures of the vortex core to cover a greater area and to shift the core outboard. There is a relatively high pressure region available for all the plan forms if the inlet were offset in the minus α direction by about 1 body diameter. A missile designed to take advantage of such a region, however, would be

limited to one-directional angle-of-attack maneuvers. The weaker vortex core of the reversed delta plan form was not visible in the schlieren photographs after it had passed through the shocks from the booster, in contrast to still being visible for the other two plan forms. The pressure surveys confirm this result in that no distinct cores are discernible for the reversed delta plan form, whereas weak vortex-core regions are shown by the contours for the straight-tipped plan forms.

CONCLUDING REMARKS

Studies of the wake behind various canard control surfaces of equal span mounted on a missile body were made at a Mach number of 1.93. The investigation revealed that reversed delta and delta control-surface plan forms gave more inboard locations of the rolled-up vortex sheet from the canard control surfaces than plan forms with straight tips. The core of the rolled-up vortex sheet was close to a location that was directly behind the tips in the free-stream direction for the straight-tipped plan forms, and was only slightly changed by angle of attack or Reynolds number for the range tested. Varying the control-surface thickness and section profile also had very little effect on the pressure field at the survey plane. The effect of simulated rocket boosters on the body was to disperse the vortex cores over a greater region and to shift them outboard. Attaching end plates to a straight-trailing-edge plan form of 0.5 taper ratio produced an outboard shift of the vortex core from the tips and did not reduce the vortex strength enough to merit the use of end plates. Raking the tips of a control surface of this plan form produced only a slight inboard shift of the vortex core.

Langley Aeronautical Laboratory,
National Advisory Committee for Aeronautics,
Langley Field, Va.

REFERENCES

1. Dryer, Murray, and Beke, Andrew: Performance Characteristics of a Normal-Shock Side Inlet Located Downstream of a Canard Control Surface at Mach numbers of 1.5 and 1.8. NACA RM E52F09, 1952.
2. Obery, Leonard J., and Krasnow, Howard S.: Influence of a Canard-Type Control Surface on the Internal and External Performance Characteristics of Nacelle-Mounted Supersonic Diffusers (Conical Centerbody) at a Rearward Body Station for a Mach Number of 2.0. NACA RM E52F16, 1952.
3. Madden, Robert T., and Kremzier, Emil J.: Data Presentation of Force Characteristics of Several Engine-Strut-Body Configurations at Mach Numbers of 1.8 and 2.0. NACA RM E51E29, 1951.
4. Wise, George A., and Dryer, Murray: Influence of a Canard-Type Control Surface on Flow Field in Vicinity of Symmetrical Fuselage at Mach Numbers 1.8 and 2.0. NACA RM E52E13, 1952.
5. Fradenburgh, Evan A., Obery, Leonard J., and Mello, John F.: Influence of Fuselage and Canard-Type Control Surface on the Flow Field Adjacent to a Rearward Fuselage Station at a Mach Number of 2.0 - Data Presentation. NACA RM E51K05, 1952.
6. Voutsas, A. M.: Parameters Involved in Selecting Final Body Profiles for Rigel XSSM-N-6 Tactical Missile. Rep. No. Aero. 19, Grumman Aircraft Eng. Corp., June 29, 1951.
7. Gracey, William, Coletti, Donald E., and Russell, Walter R.: Wind-Tunnel Investigation of a Number of Total-Pressure Tubes at High Angles of Attack. Supersonic Speeds. NACA TN 2261, 1951.



Figure 1.- Test setup showing model with the 30° raked-tips canard control surface installed.

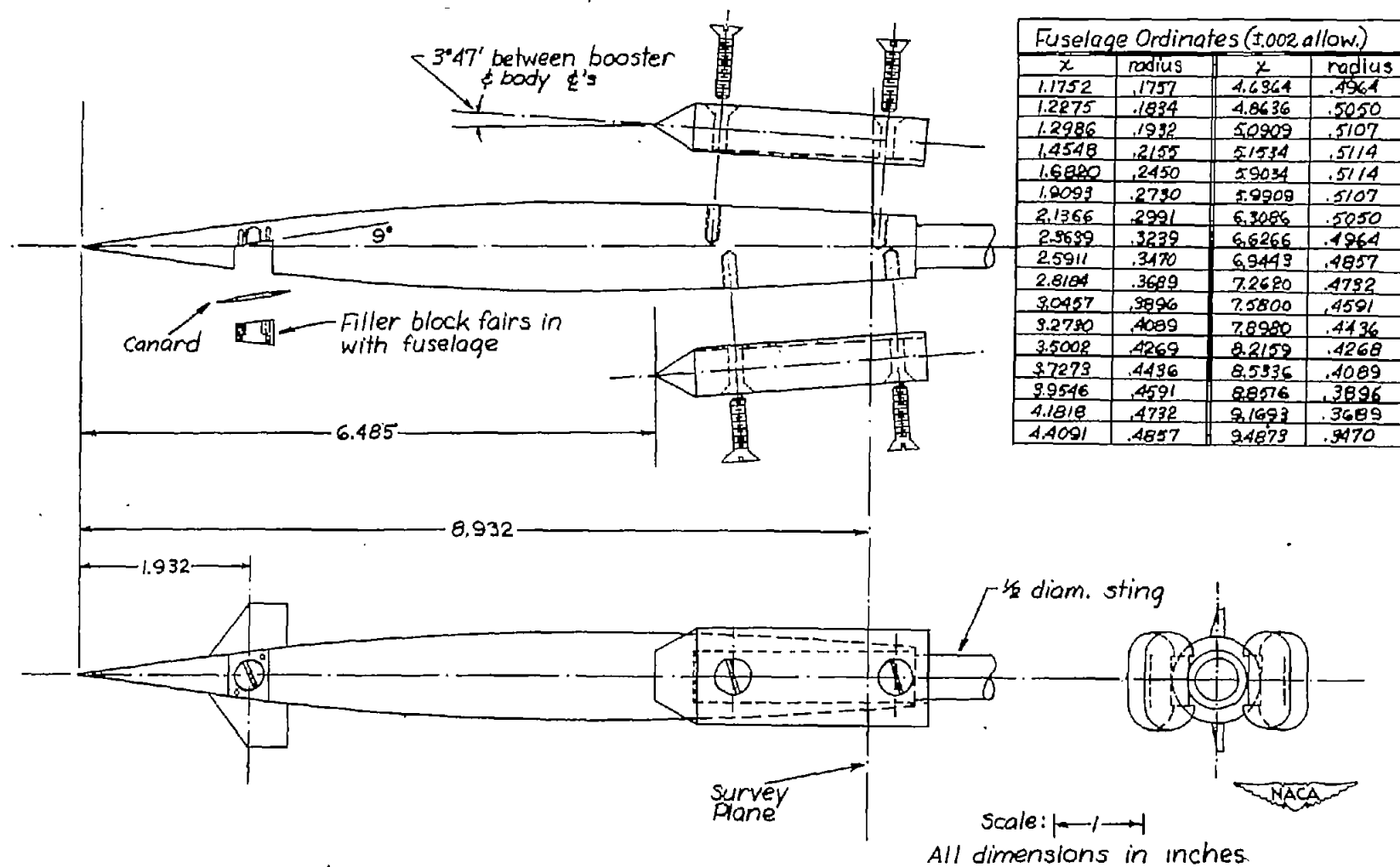
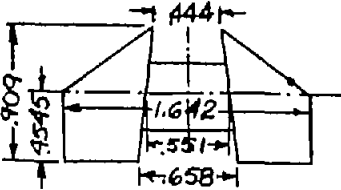
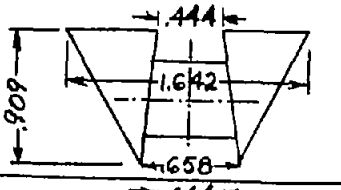
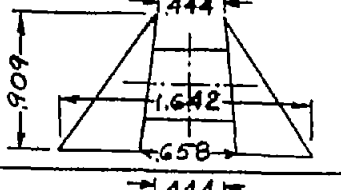
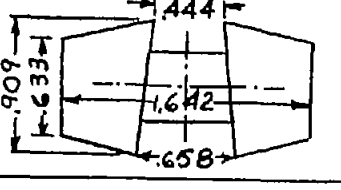


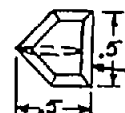
Figure 2.- Sketch of model.

PLANFORMS	CONFIG. NO.	DESCRIPTION
	1.	A 0.5 taper ratio; 8 percent thick; modified circular-arc section.* B 0.5 taper ratio; 8 percent thick; hexagonal section.** C 0.5 taper ratio; 4 percent thick; hexagonal section.** D Same as 1A except with boosters. E Same as 1A except with end plates.*** F Same as 1A except with 30° raked tips.
	2.	A Reversed delta; 4 percent thick, hexagonal section.** B Same as 2A except with boosters.
	3.	A Point-forward delta; 4 percent thick; hexagonal section.**
	4.	A 0.697 taper ratio; 8 percent thick; hexagonal section.** B 0.697 taper ratio; 4 percent thick; hexagonal section.** C Same as 4A except with boosters.

* Leading and trailing edges are wedge sections, tangent to the circular-arc section at 25 and 75 percent chord.

** Flat plate with leading- and trailing-edge wedge section over forward and rearward 25 percent chord.

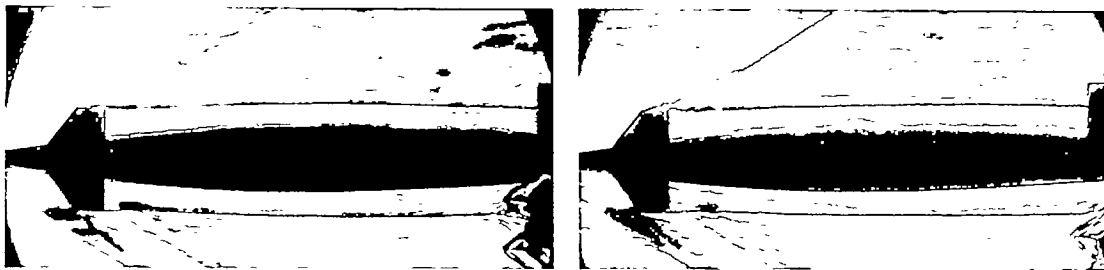
*** End-plate detail:



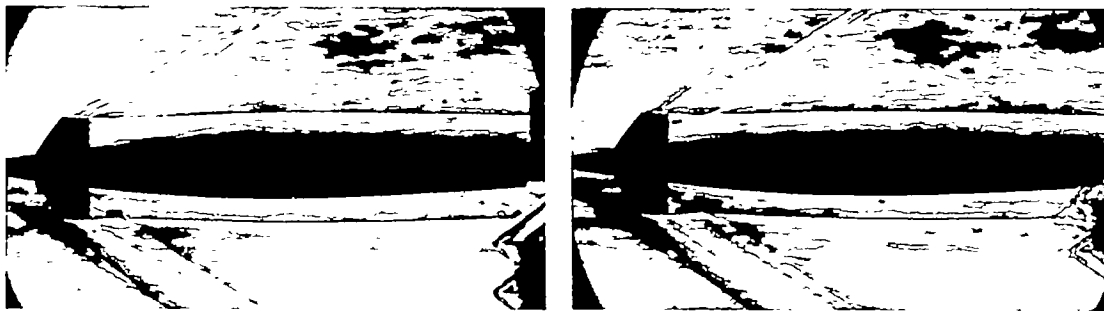
0.015 thick, beveled on the outside.



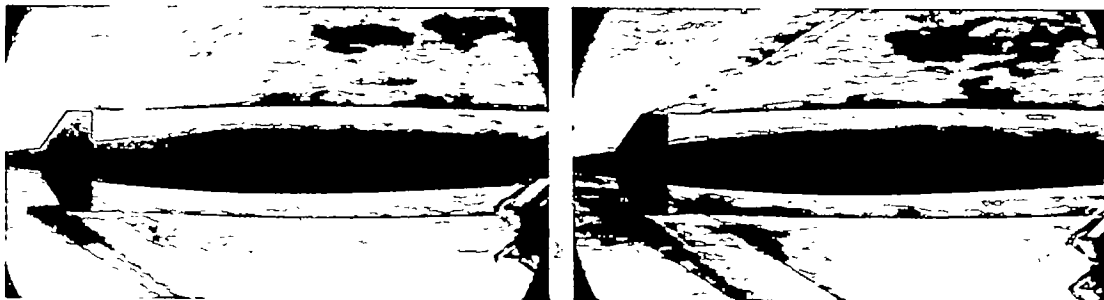
Figure 3.- Sketch of various control surfaces investigated.

 $Q = 0^\circ$ $Q = 35^\circ$

(a) Control surface 1A (0.5 taper, straight trailing edge, 8-percent modified circular-arc section).

 $Q = 0^\circ$ $Q = 35^\circ$

(b) Control surface 1B (0.5 taper, straight trailing edge, 8-percent hexagonal section).

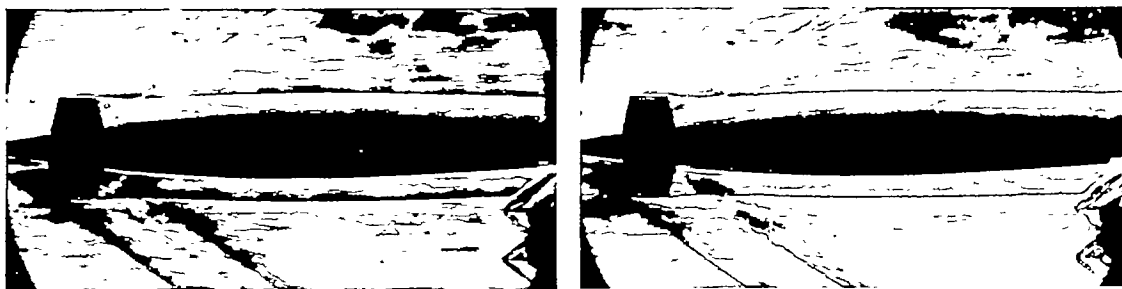
 $Q = 0^\circ$ $Q = 35^\circ$

(c) Control surface 1C (0.5 taper, straight trailing edge, 4-percent hexagonal section).

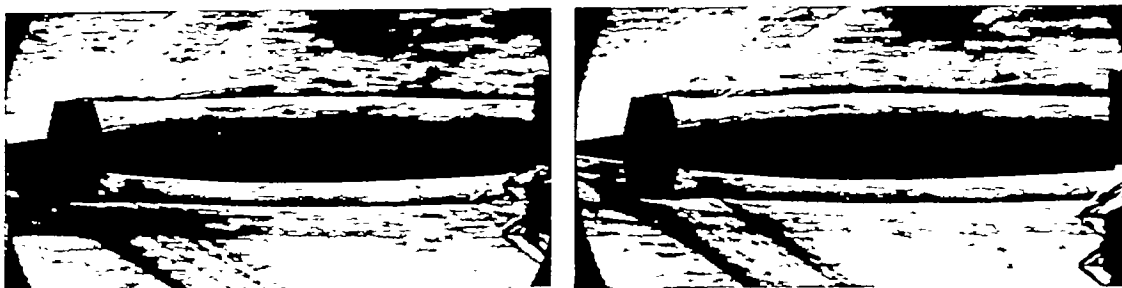


L-76950

Figure 4.- Schlieren photographs illustrating the paths of the core of the rolled-up vortex sheet with distance downstream for the various canard control surfaces.

 $\alpha = 0^\circ$ $\alpha = 35^\circ$

(d) Control surface 4A (0.697 straight taper, 8-percent hexagonal section).

 $\alpha = 0^\circ$ $\alpha = 35^\circ$

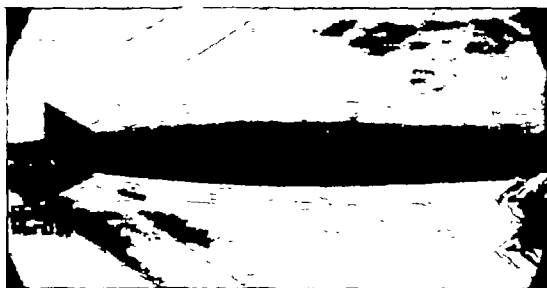
(e) Control surface 4B (0.697 straight taper, 4-percent hexagonal section).

 $\alpha = 0^\circ$ $\alpha = 35^\circ$

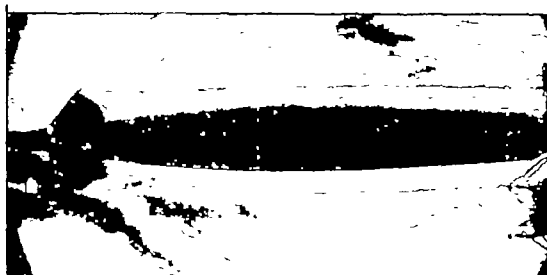
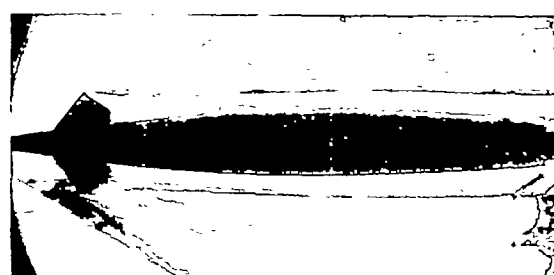
(f) Control surface 3A (point-forward delta, 4-percent hexagonal section).

Figure 4.- Continued.

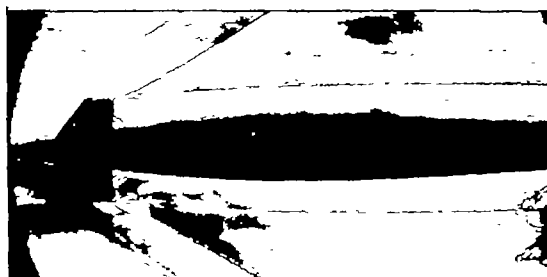
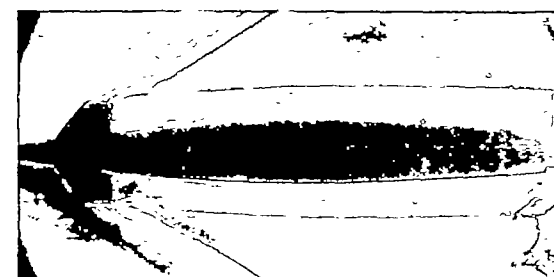
NACA
L-76951

 $\alpha = 0^\circ$  $\alpha = 35^\circ$

(g) Control surface 2A (reversed delta, 4-percent hexagonal section).

 $\alpha = 0^\circ$  $\alpha = 3.5^\circ$

(h) Control surface 1F (control surface 1A except with 30° raked tips).

 $\alpha = 0^\circ$  $\alpha = 35^\circ$

(i) Control surface 1E (control surface 1A except with end plates).

Figure 4.- Continued.

NACA
L-76952

 $\alpha = 0^\circ$ $\alpha = 3.5^\circ$

(j) Control surface 1D (control surface 1A except with boosters on the body).

 $\alpha = 0^\circ$ $\alpha = 3.5^\circ$

(k) Control surface 4C (control surface 4A except with boosters on the body).

 $\alpha = 0^\circ$ $\alpha = 3.5^\circ$

(l) Control surface 2B (control surface 2A except with boosters on the body).

Figure 4.- Concluded.

NACA
L-76953

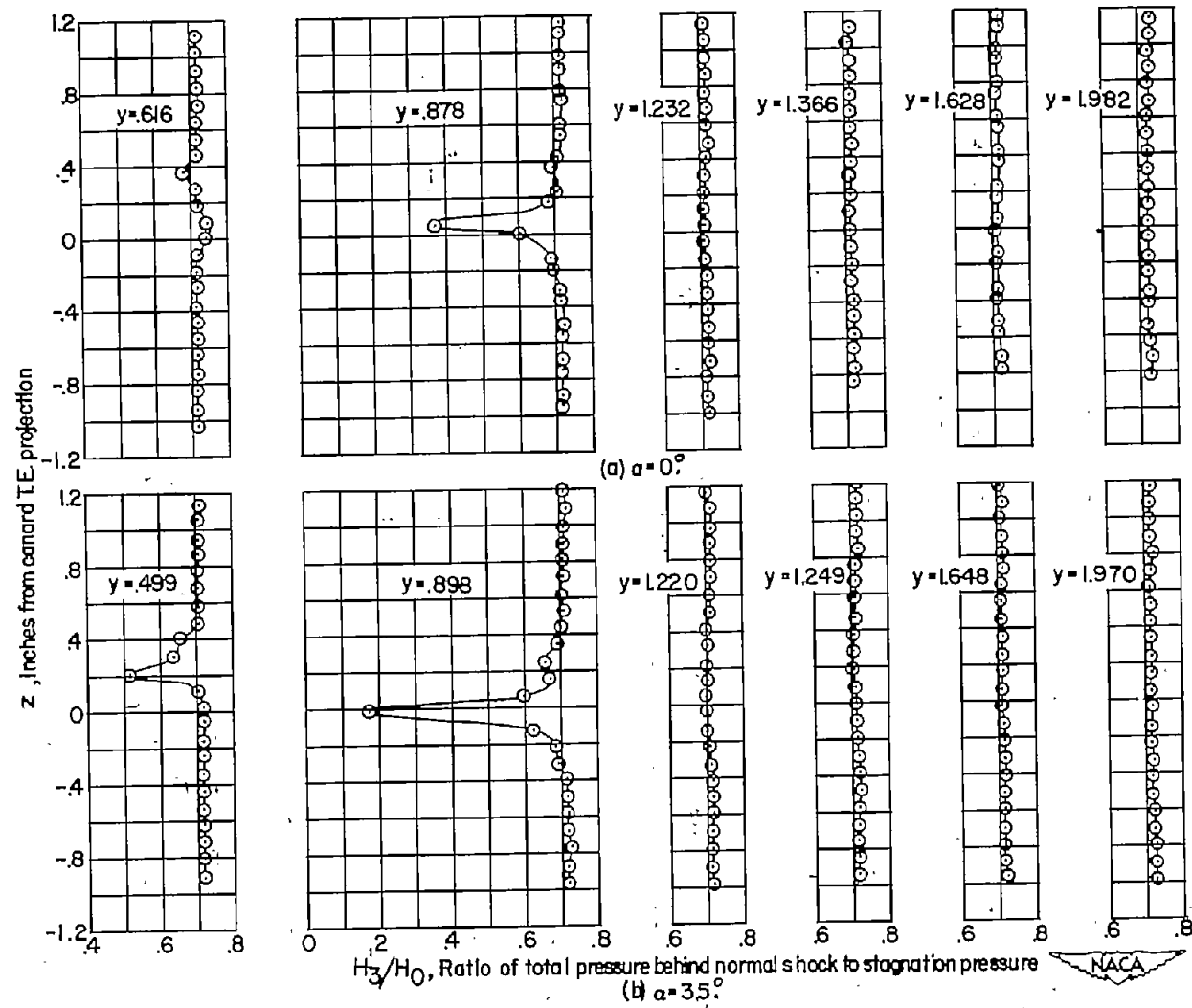


Figure 5.- Wake profiles behind control surface 1A (0.5 taper, 8-percent modified circular-arc section).

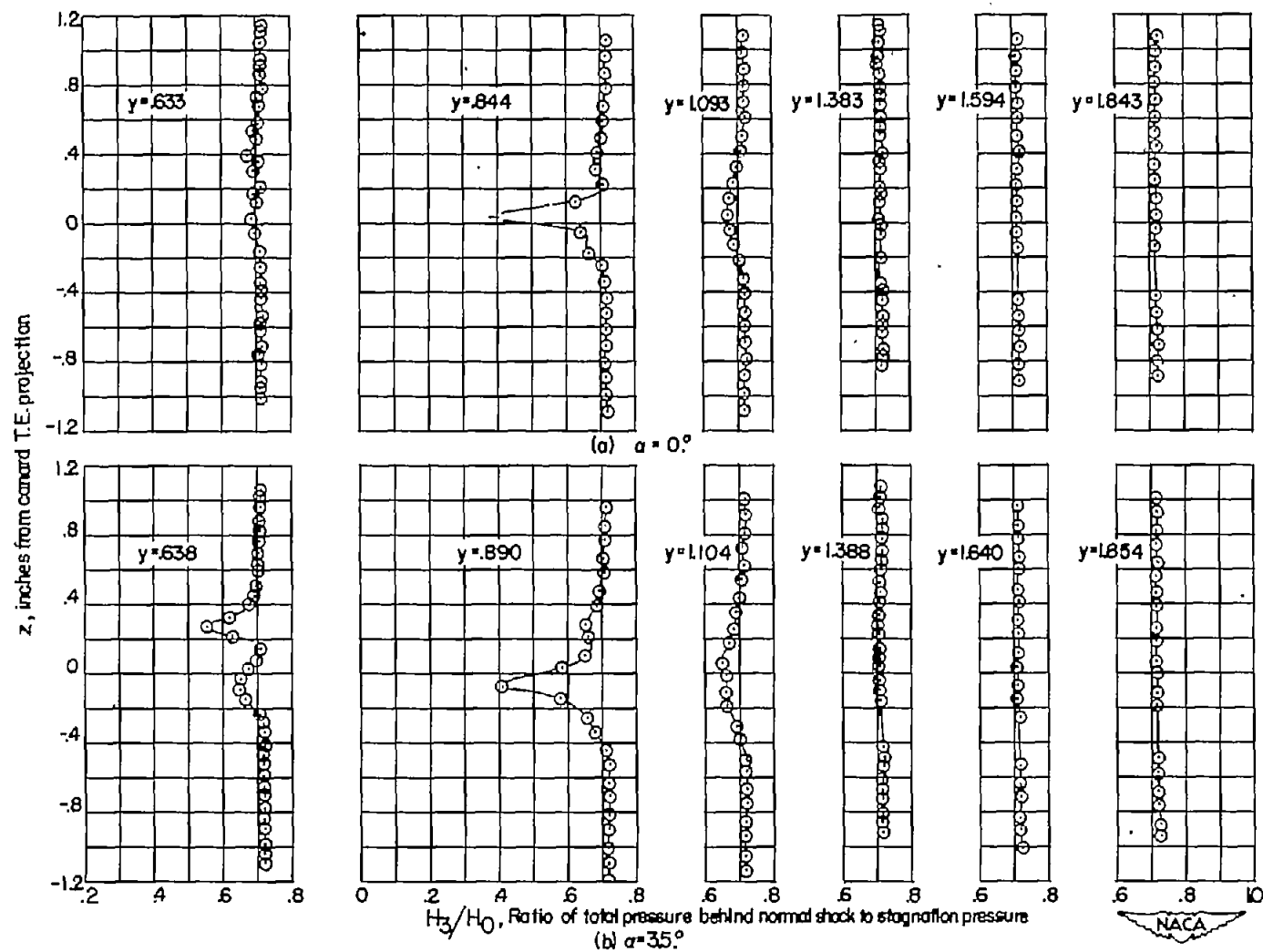


Figure 6.- Wake profiles behind control surface 4A (0.697 taper, 8-percent hexagonal section).

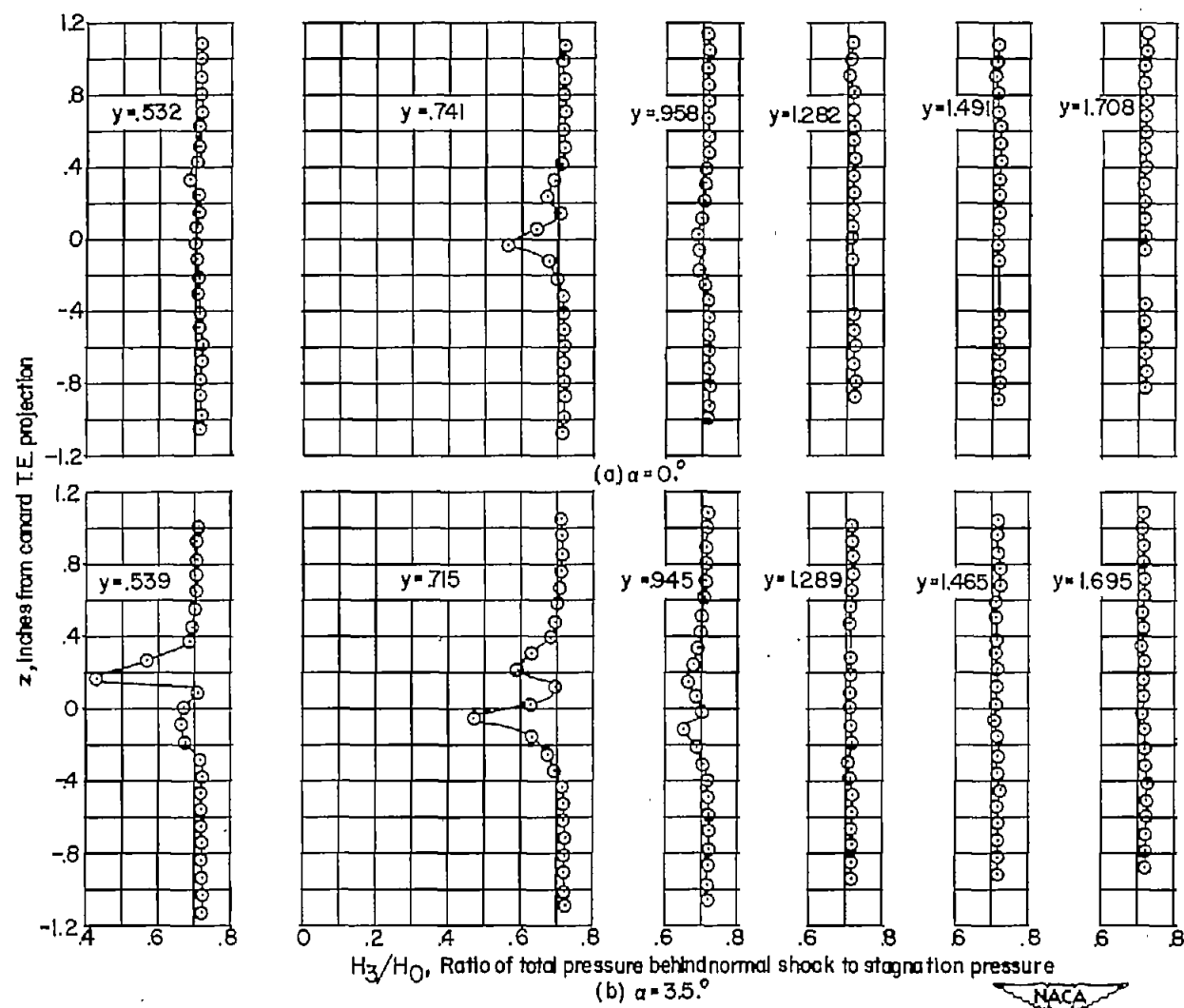


Figure 7.- Wake profiles behind control surface 2A (reversed delta, 4-percent hexagonal section).

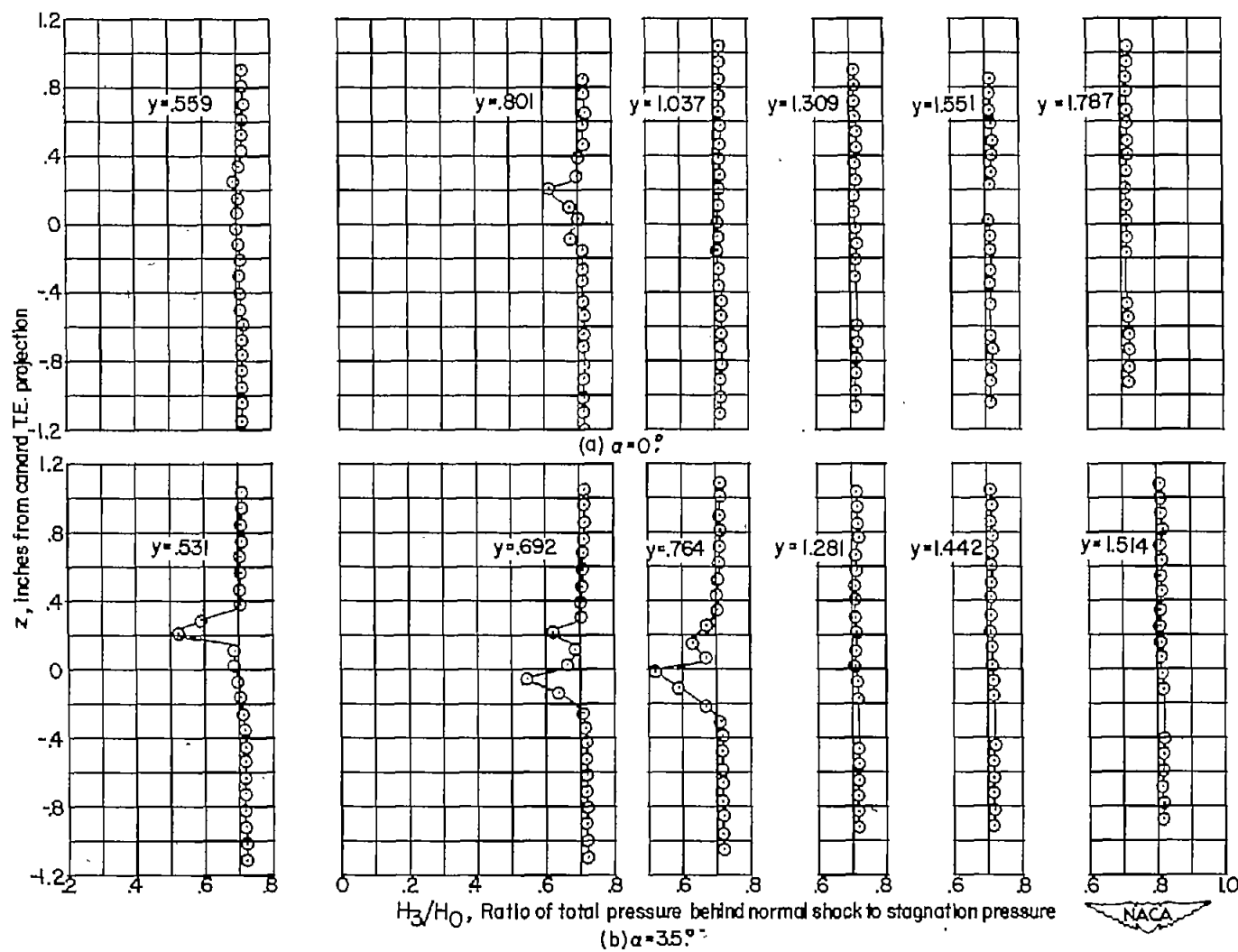


Figure 8.- Wake profiles behind control surface 3A (point-forward delta, 4-percent hexagonal section).

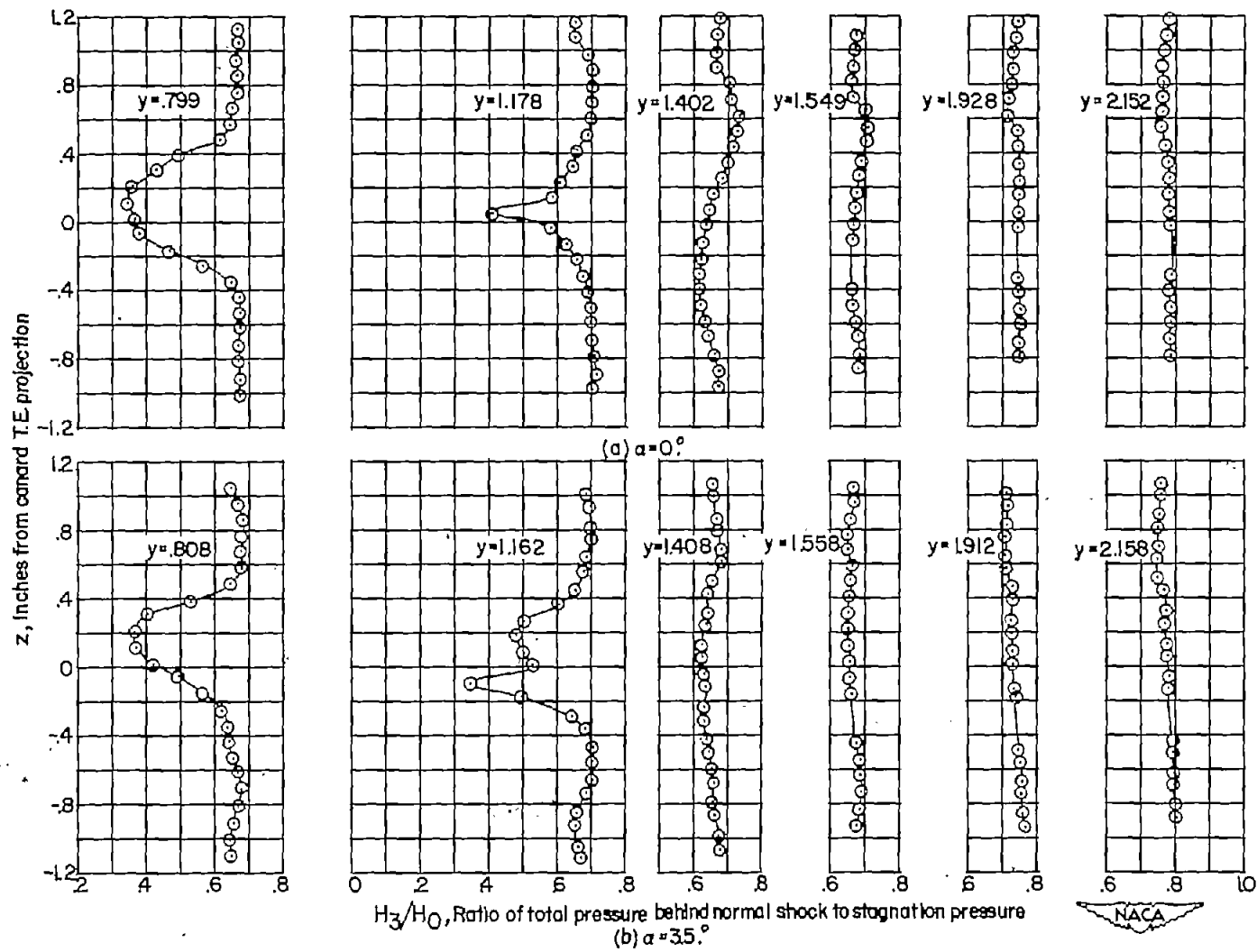
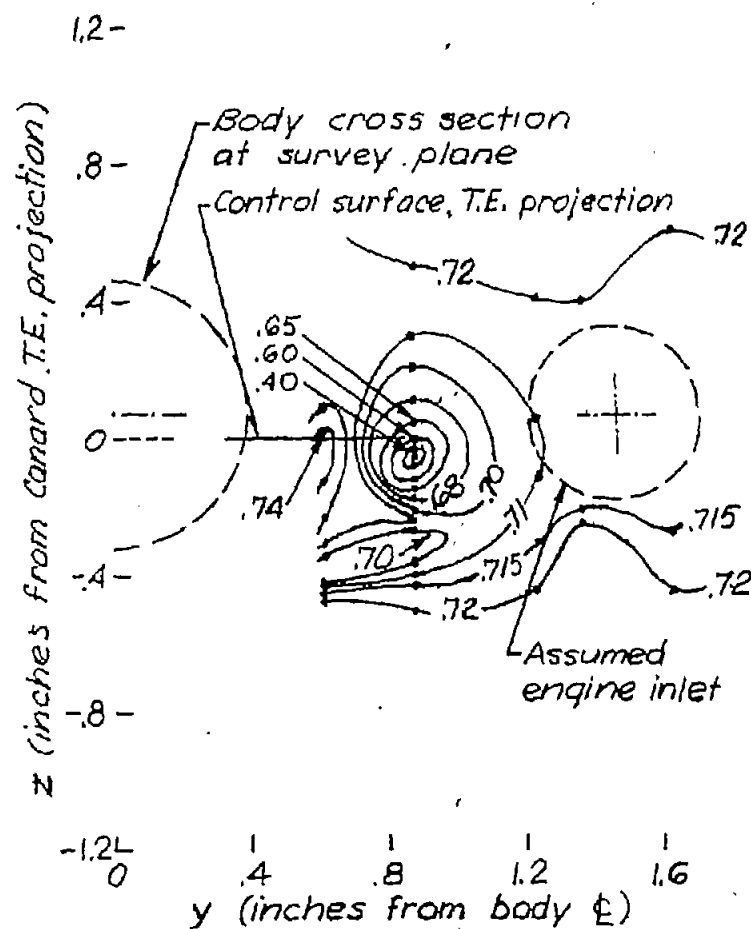
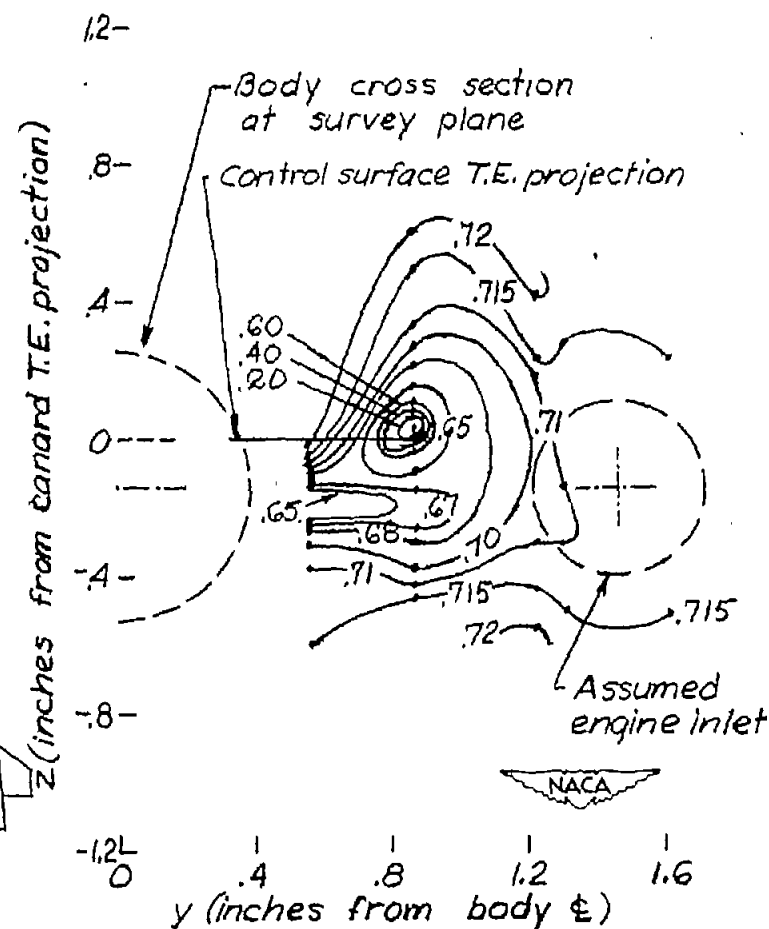


Figure 9.- Wake profile behind control surface 1D (same as 1A except with boosters on body).

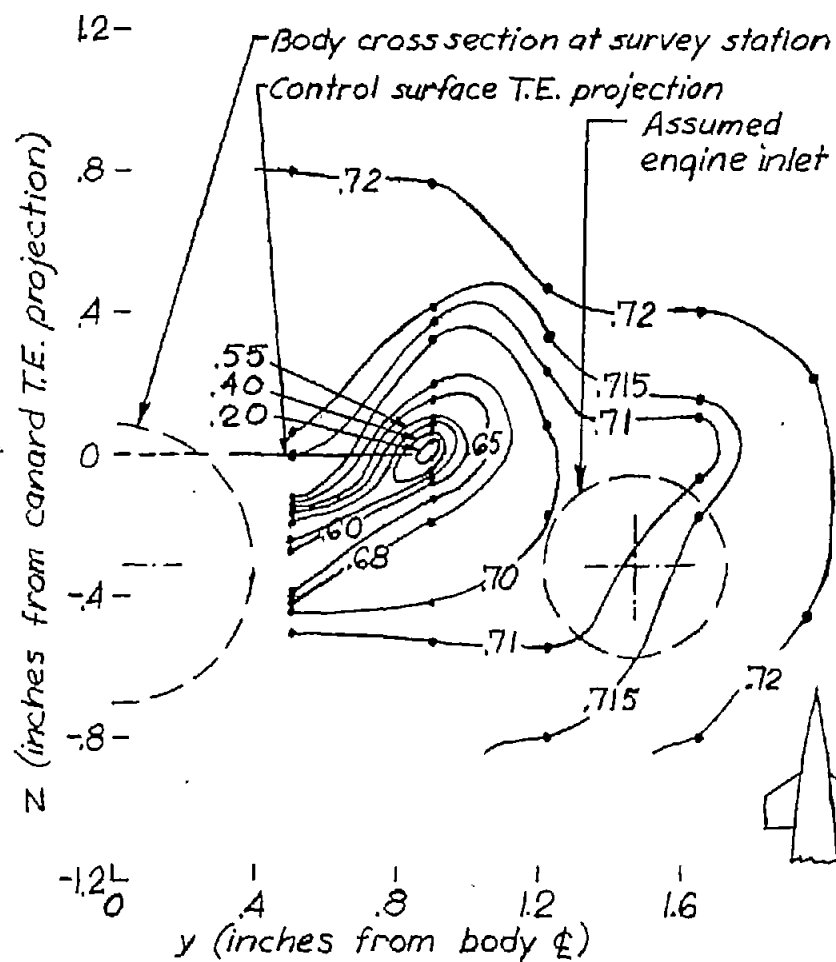


(a) $\alpha = 0^\circ$; $H_0 = 114.7 \text{ in. Hg abs.}$

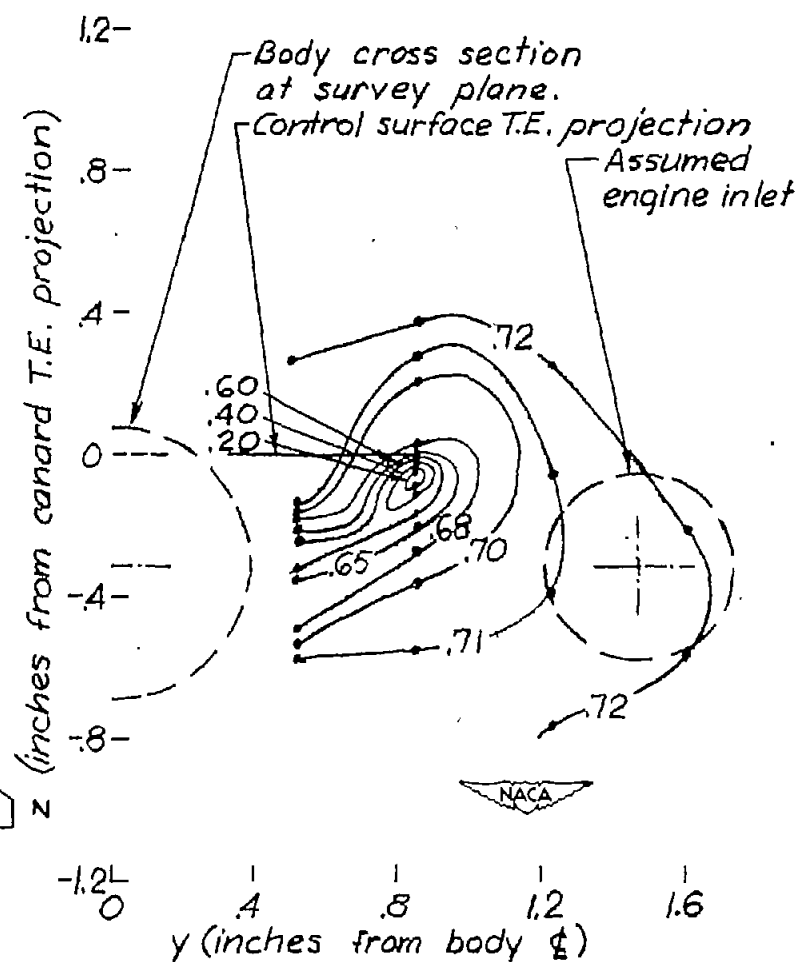


(b) $\alpha = 2^\circ$; $H_0 = 114.7 \text{ in. Hg abs.}$

Figure 10.- Contours for the values of H_3/H_0 behind control surface 1A (0.5 λ , straight trailing edge, 8-percent modified circular-arc section).

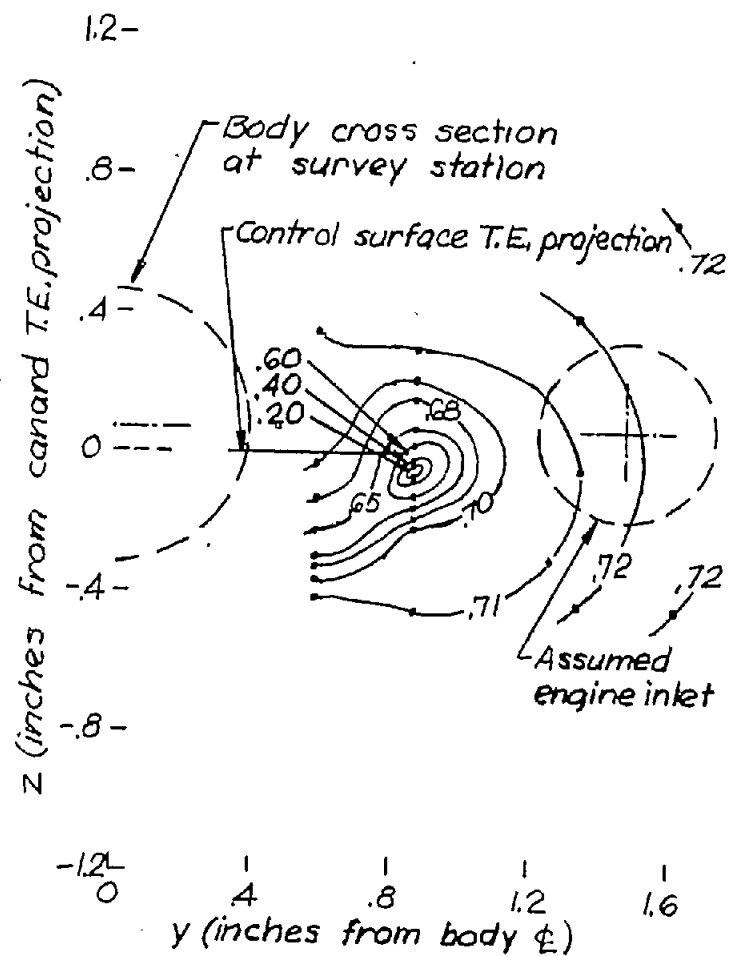


(c) $\alpha = 3.5^\circ$; $H_0 = 114.7 \text{ in. Hg abs.}$

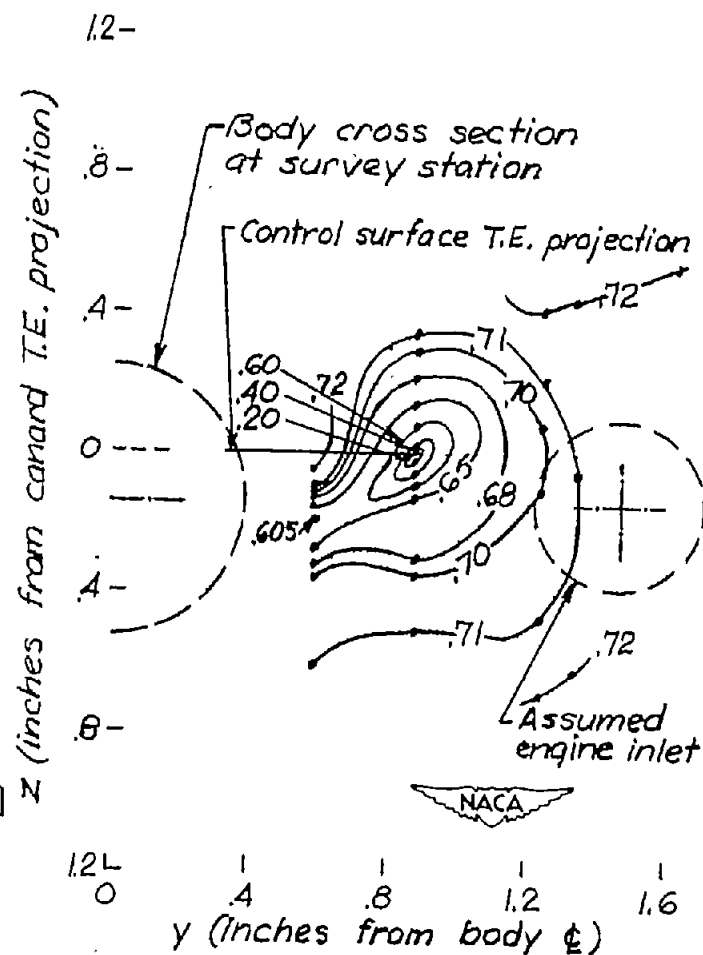


(d) $\alpha = 3.5^\circ$; $H_0 = 31.0 \text{ in. Hg abs.}$

Figure 10.- Concluded.

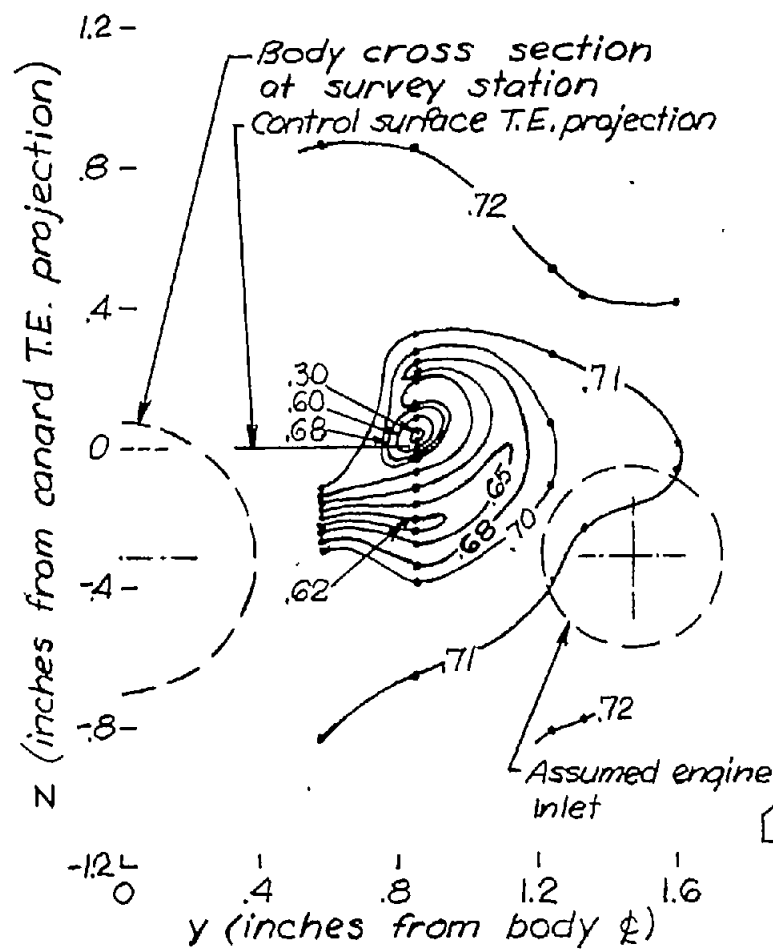


(a) $\alpha = 0^\circ$; $H_0 = 114.3 \text{ in. } Hq \text{ abs.}$

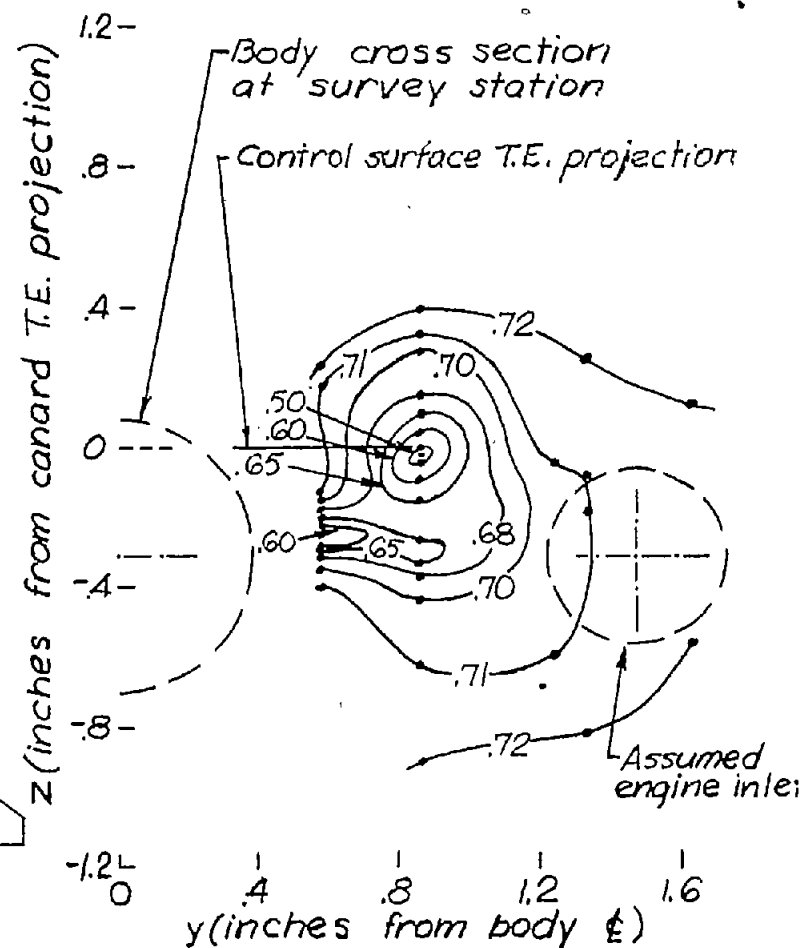


(b) $\alpha = 2^\circ$; $H_0 = 114.3 \text{ in. } Hq \text{ abs.}$

Figure 11.- Contours for the values of H_3/E_0 behind control surface 1B (0.5λ , straight trailing edge, 8-percent hexagonal section).

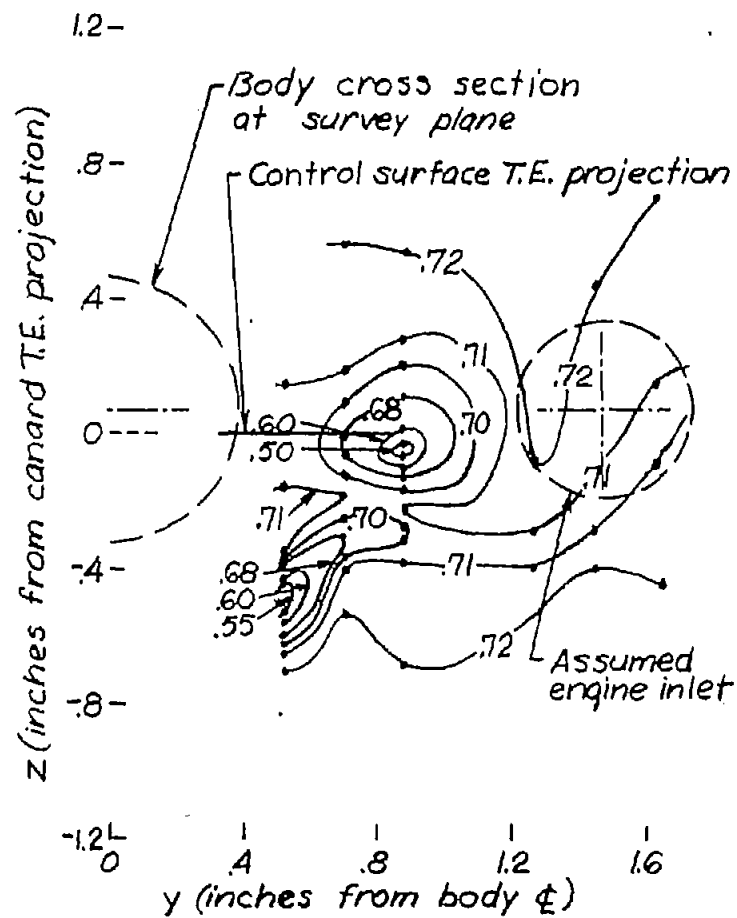


(c) $\alpha = 3.6^\circ$; $H_0 = 114.2 \text{ in. Hg abs.}$

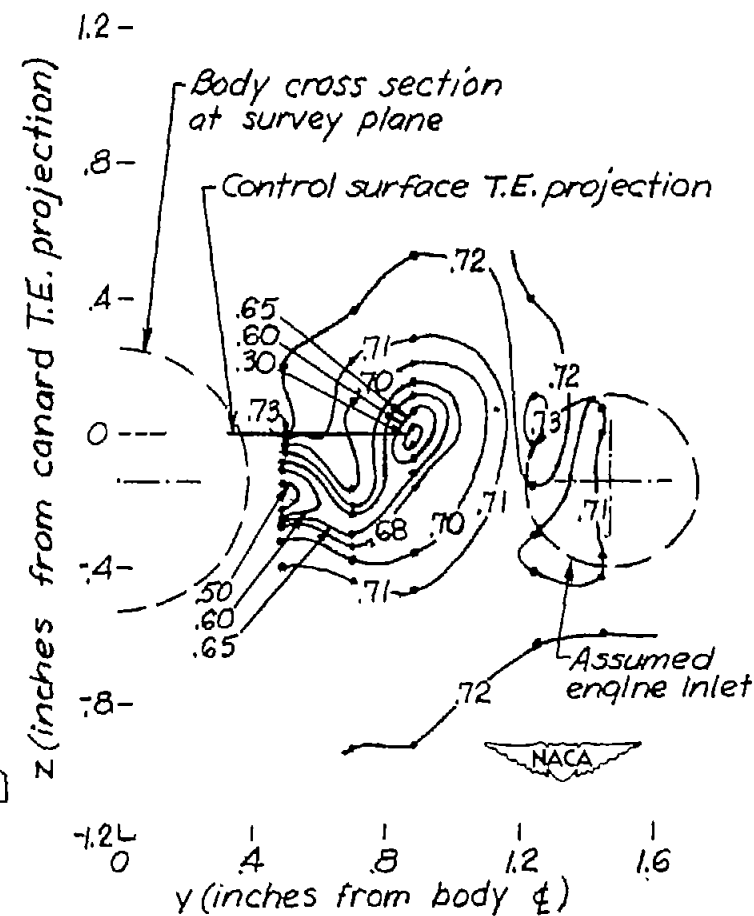


(d) $\alpha = 3.6^\circ$; $H_0 = 31.6 \text{ in. Hg abs.}$

Figure 11.- Concluded.

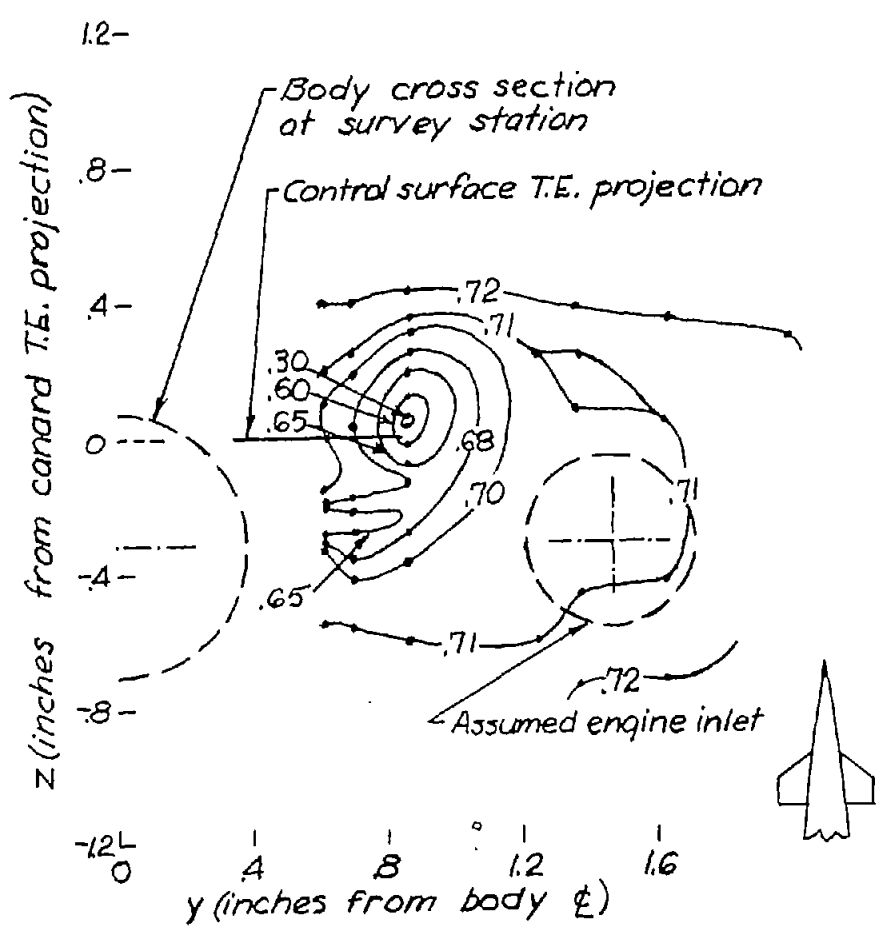


(a) $\alpha = 0^\circ$; $H_0 = 114.3$ in. H_q abs.

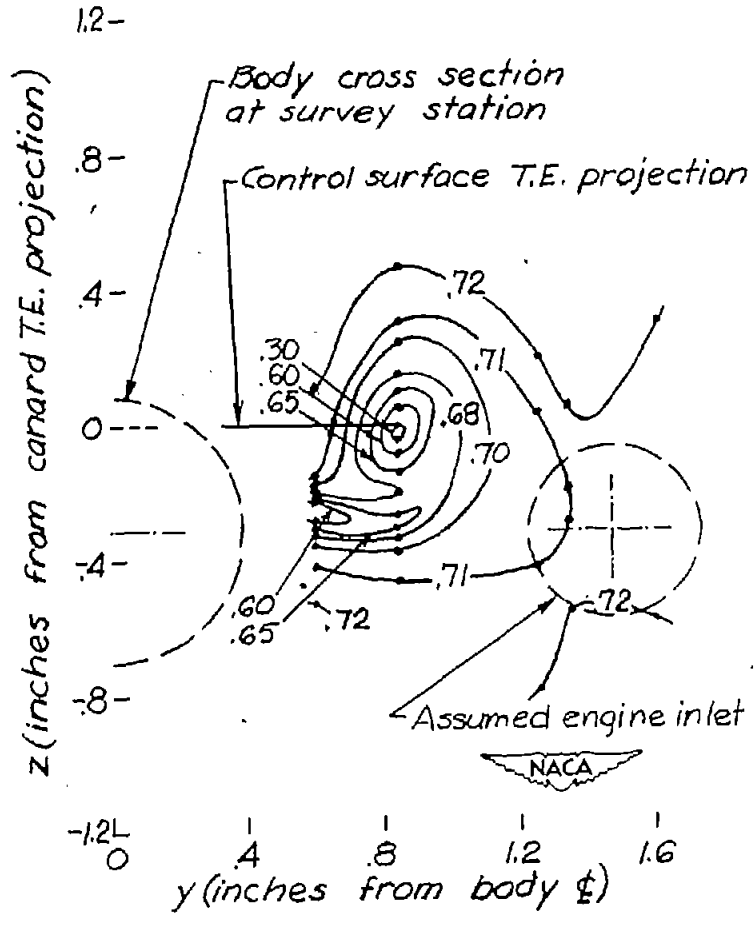


(b) $\alpha = 2^\circ$; $H_0 = 114.6$ in. H_q abs.

Figure 12.- Contours for the values of H_3/H_0 behind control surface 1C
(0.5λ , straight trailing edge, 4-percent hexagonal section).

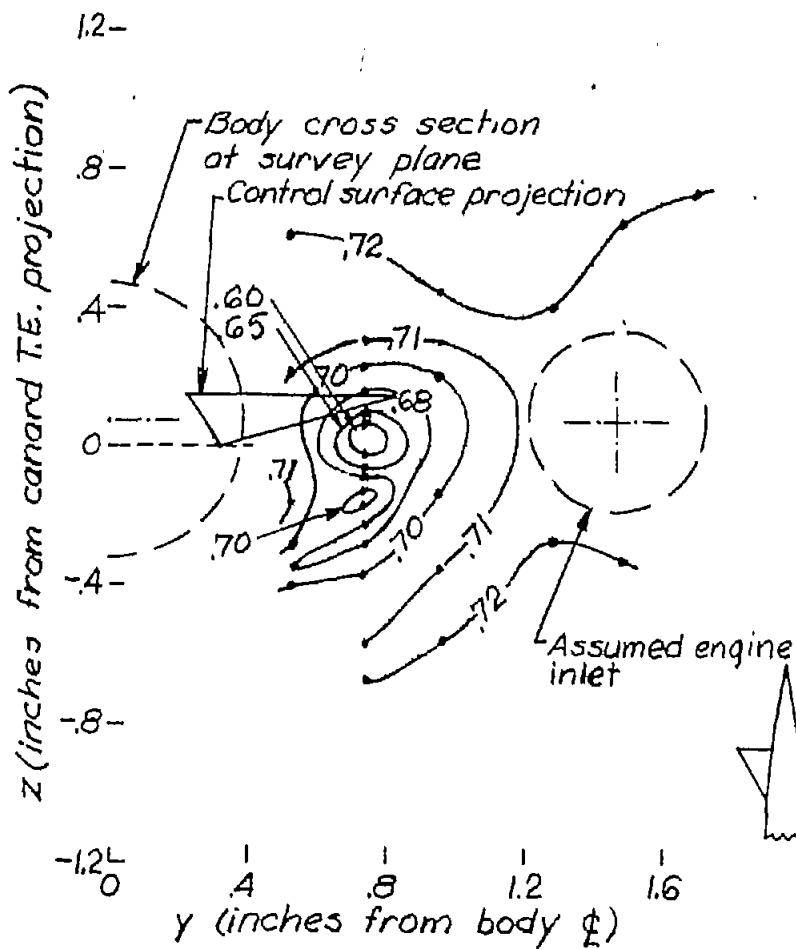


(c) $\alpha = 3.5^\circ$; $H_0 = 114.4$ in. Hg abs.

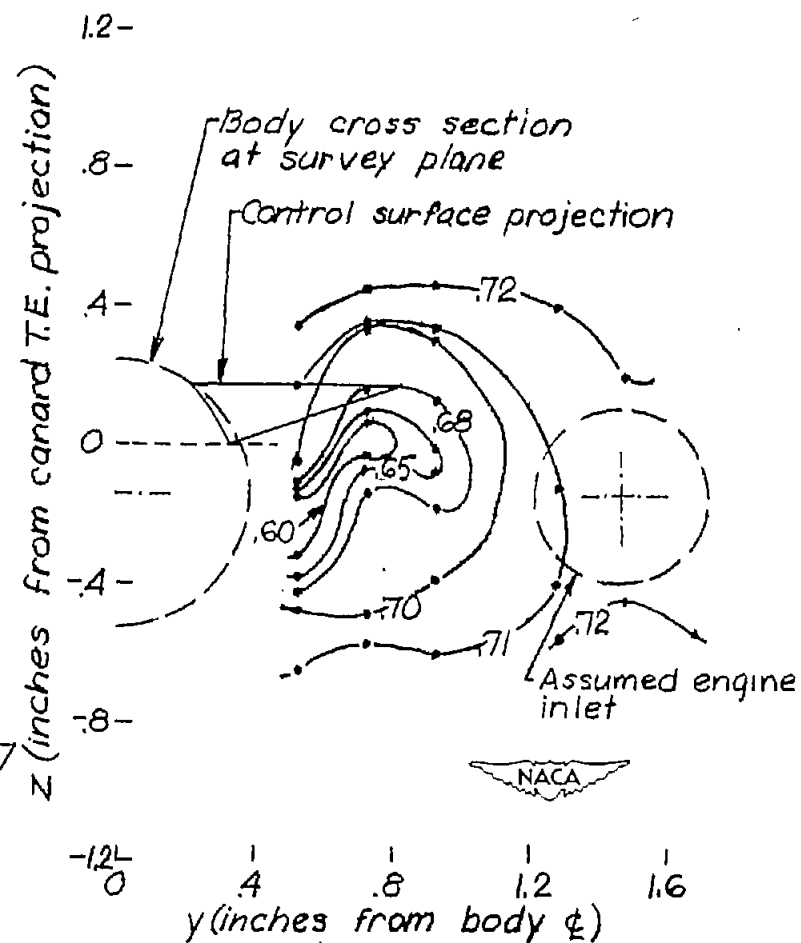


(d) $\alpha = 3.5^\circ$; $H_0 = 30.9$ in. Hg abs.

Figure 12.- Concluded.

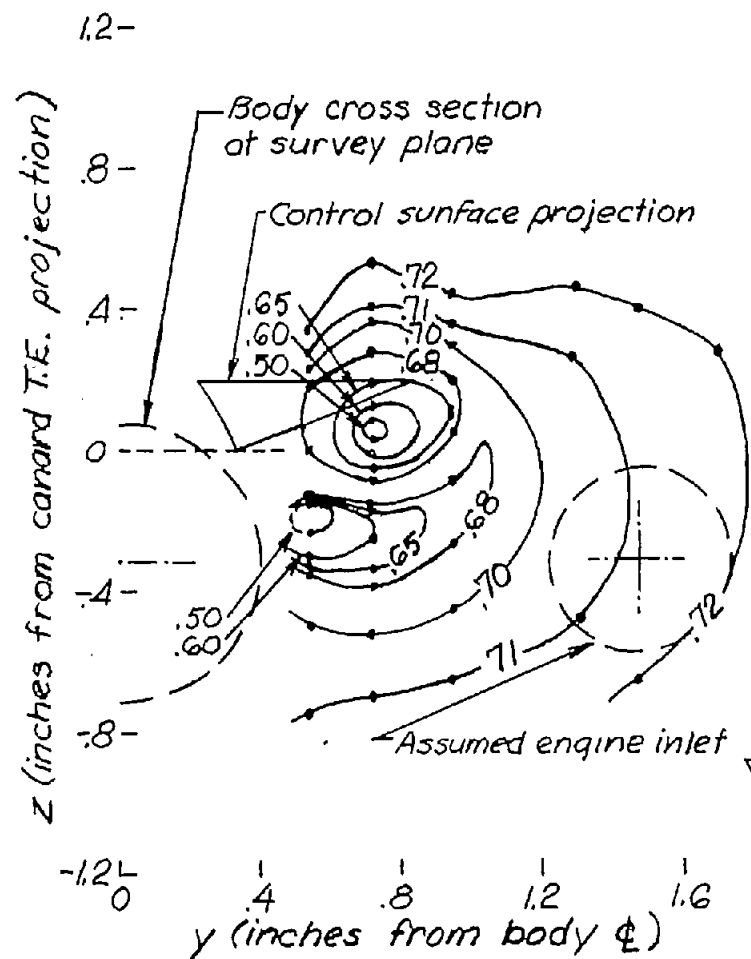


(a) $\alpha = 0^\circ$; $H_0 = 114.6$ in.Hg. abs.

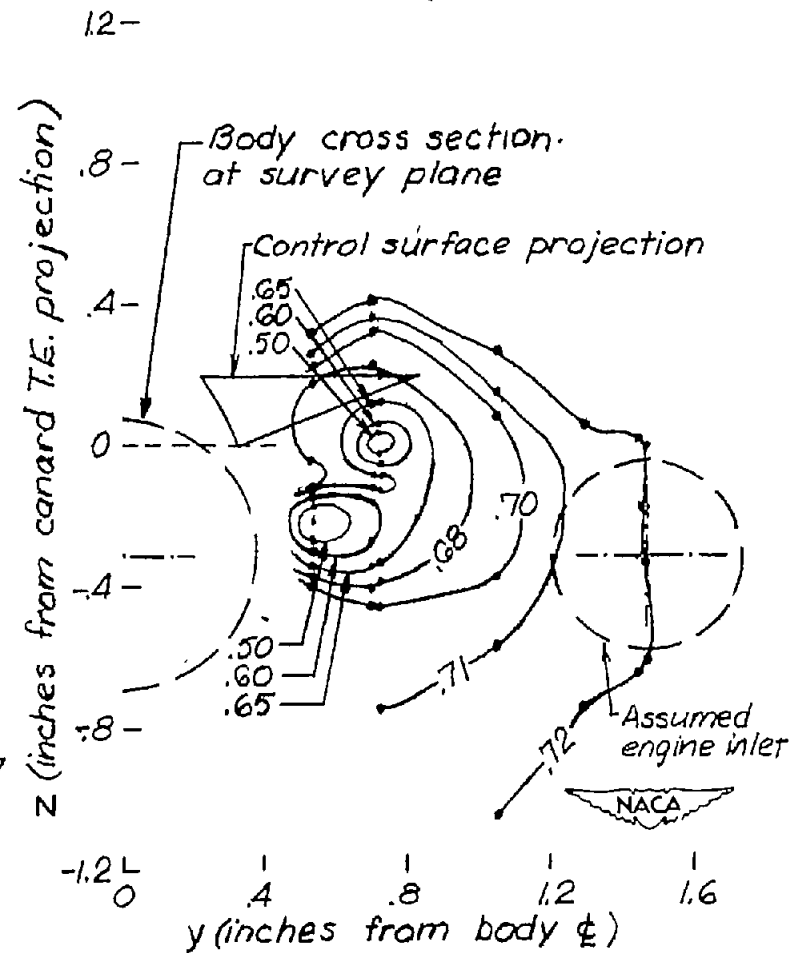


(b) $\alpha = 2^\circ$; $H_0 = 114.6$ in.Hg. abs.

Figure 13.- Contours for the values of H_3/H_0 behind control surface 2A (reversed delta, 4-percent hexagonal section).

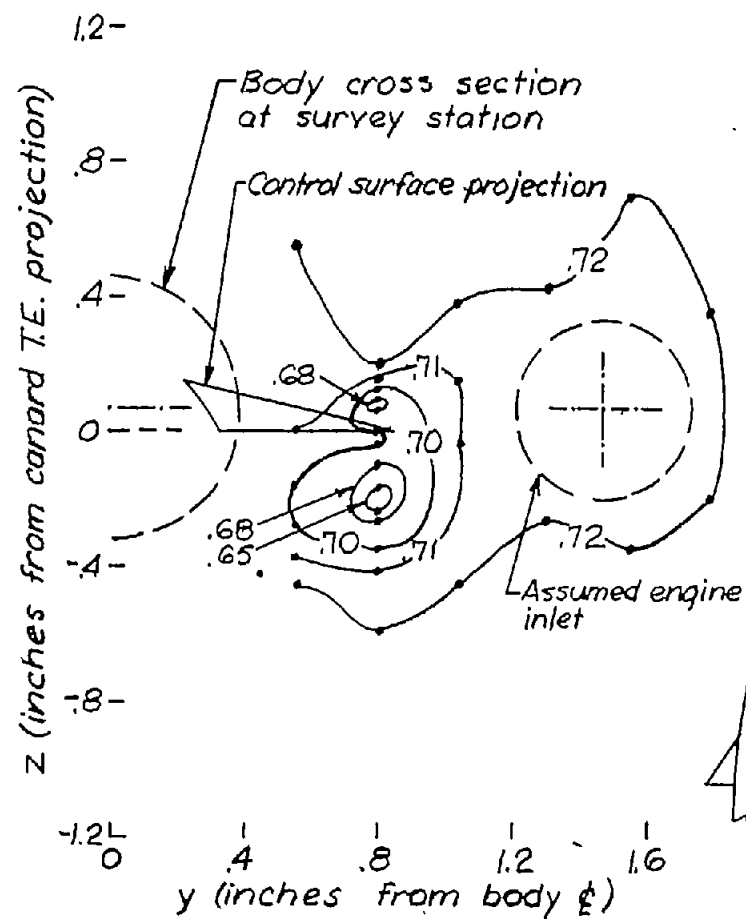


(c) $\alpha = 3.5^\circ$; $H_0 = 114.6$ in. Hg abs.

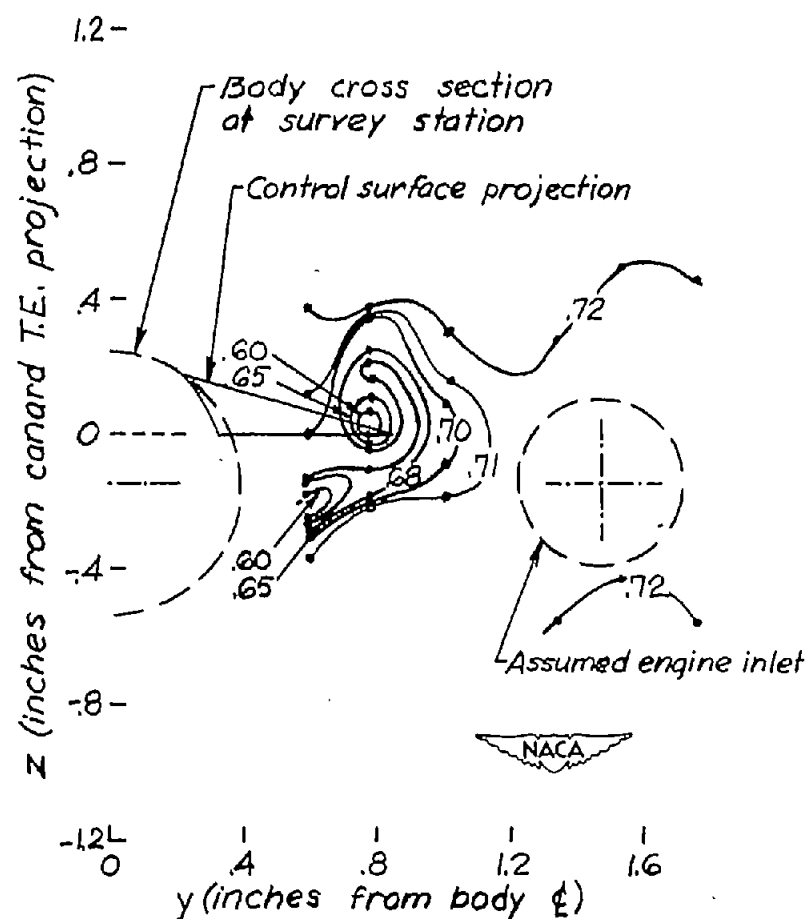


(d) $\alpha = 3.5^\circ$; $H_0 = 31.5$ in. Hg abs.

Figure 13.- Concluded.

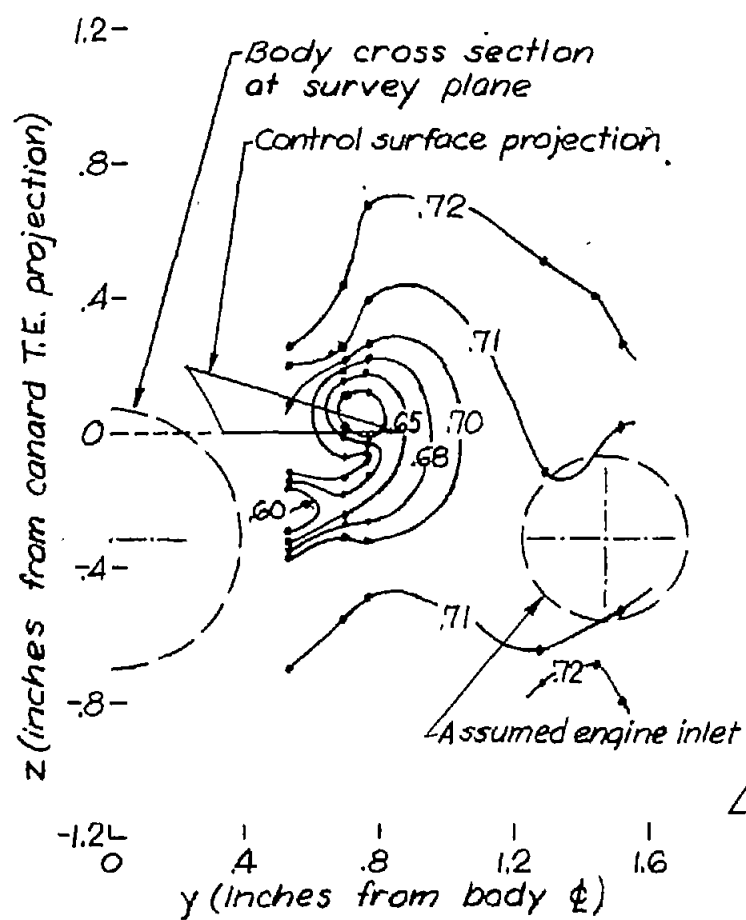


(a) $\alpha = 0^\circ$; $H_0 = 115.0$ in. Hg abs.

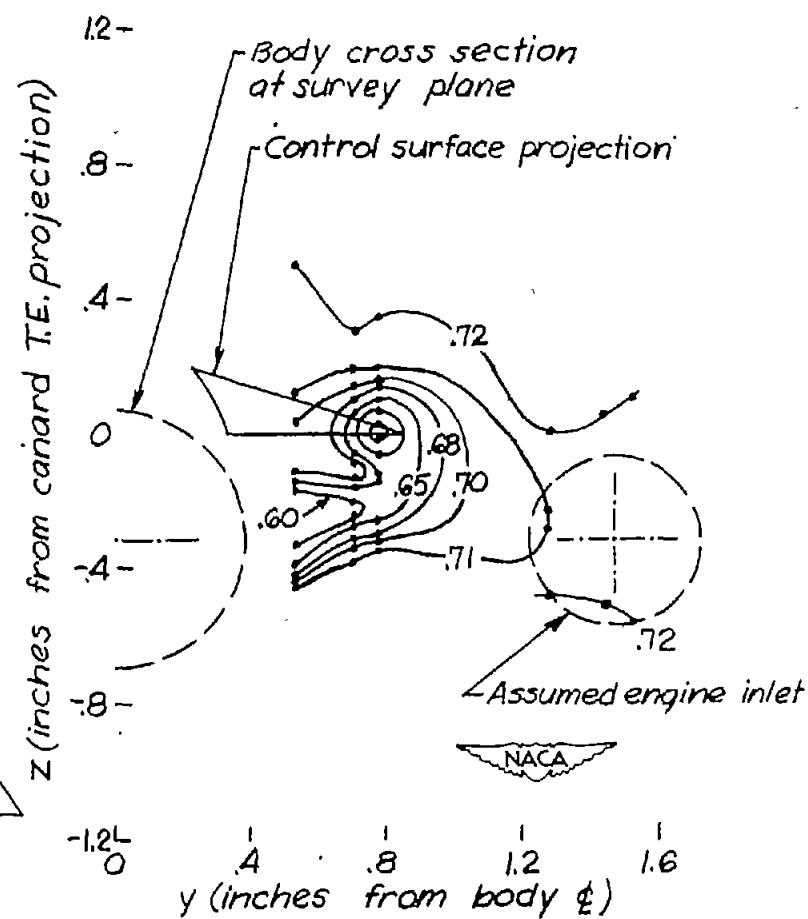


(b) $\alpha = 2^\circ$; $H_0 = 114.7$ in. Hg abs.

Figure 14.- Contours for the values of H_3/H_0 behind control surface 3A (point-forward delta, 4-percent hexagonal section).

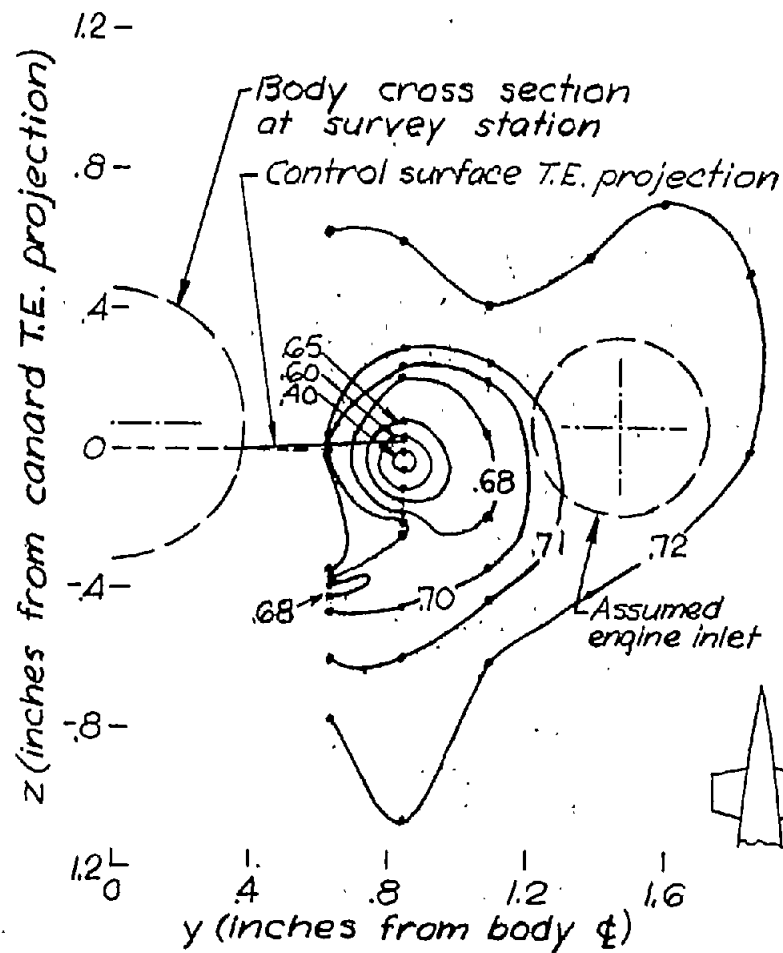


(c) $\alpha = 3.5^\circ$; $H_0 = 114.7$ in. Hg abs.

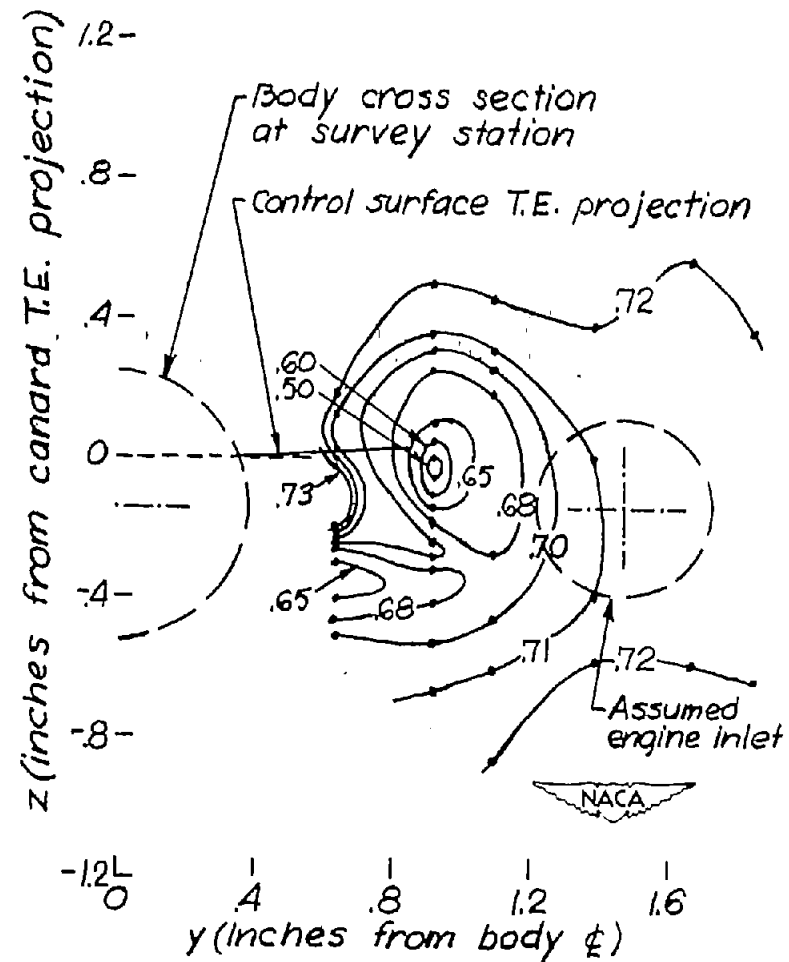


(d) $\alpha = 3.5^\circ$; $H_0 = 31.1$ in. Hg abs.

Figure 14.- Concluded.

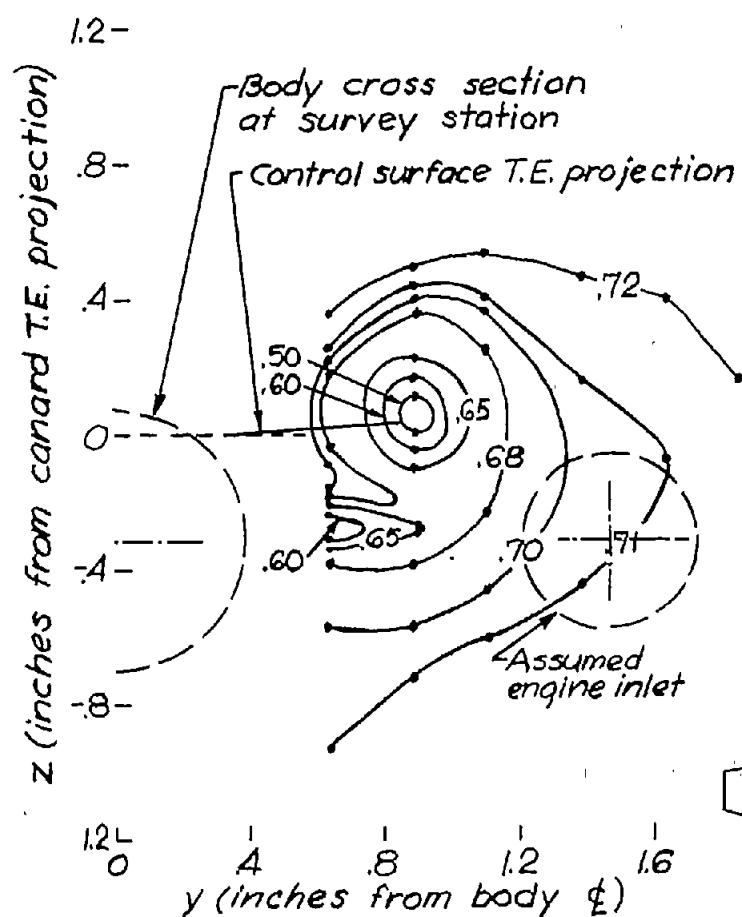


(a) $\alpha = 0^\circ$; $H_0 = 114.3 \text{ in. } H_q \text{ abs.}$

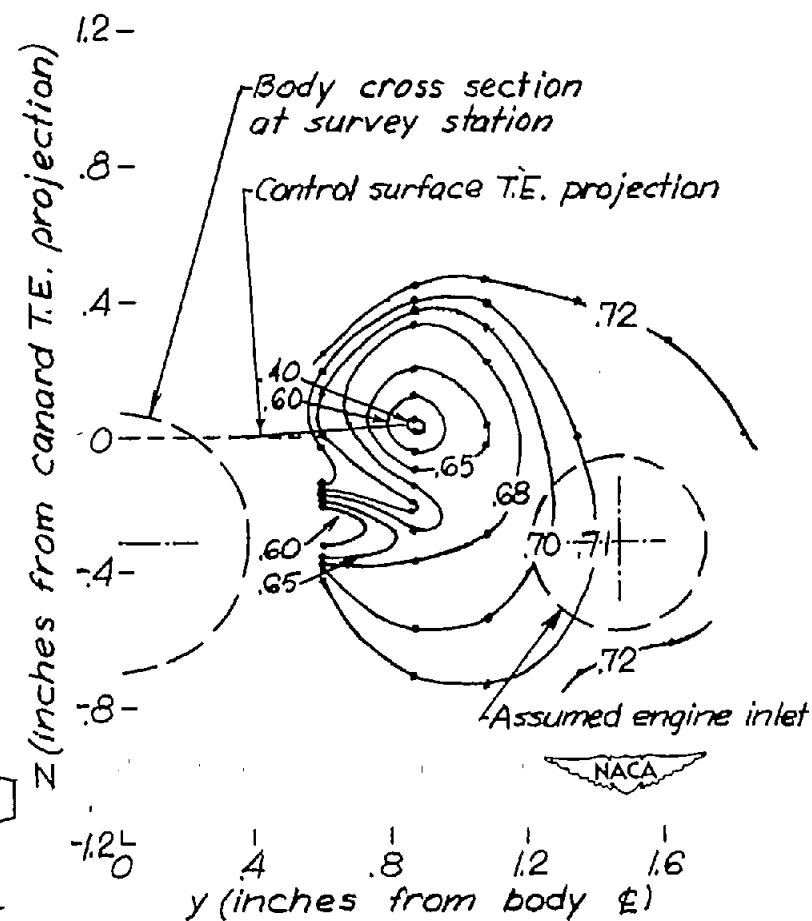


(b) $\alpha = 2^\circ$; $H_0 = 114.4 \text{ in. } H_q \text{ abs.}$

Figure 15.- Contours for the values of H_3/H_0 behind control surface 4A
(0.697 straight taper, 8-percent hexagonal section).

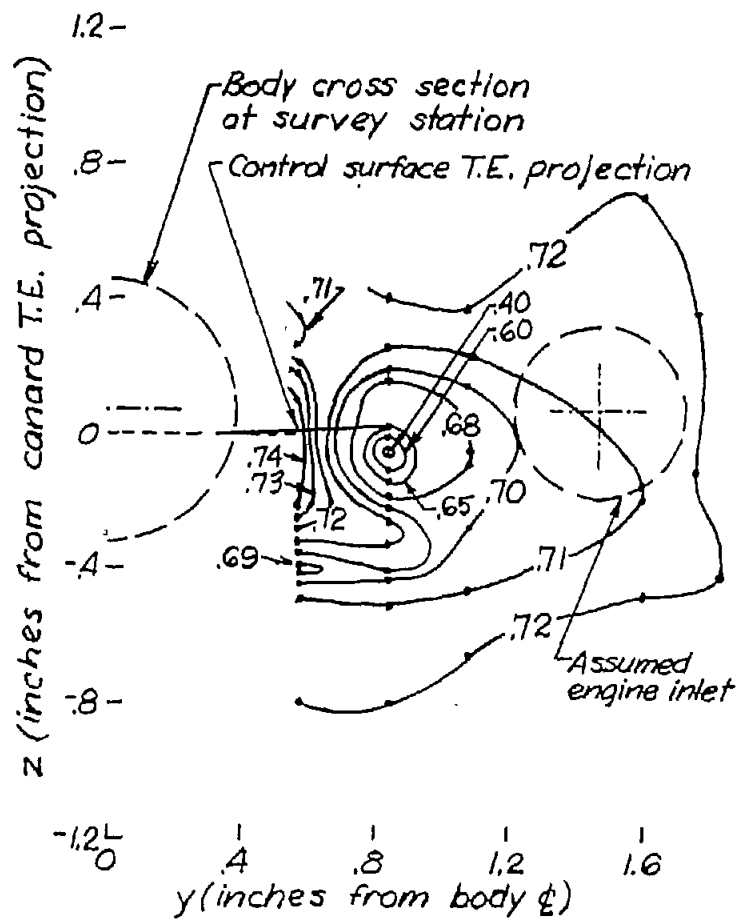


(c) $\alpha = 3.5^\circ$; $H_0 = 114.4$ in. Hg abs.

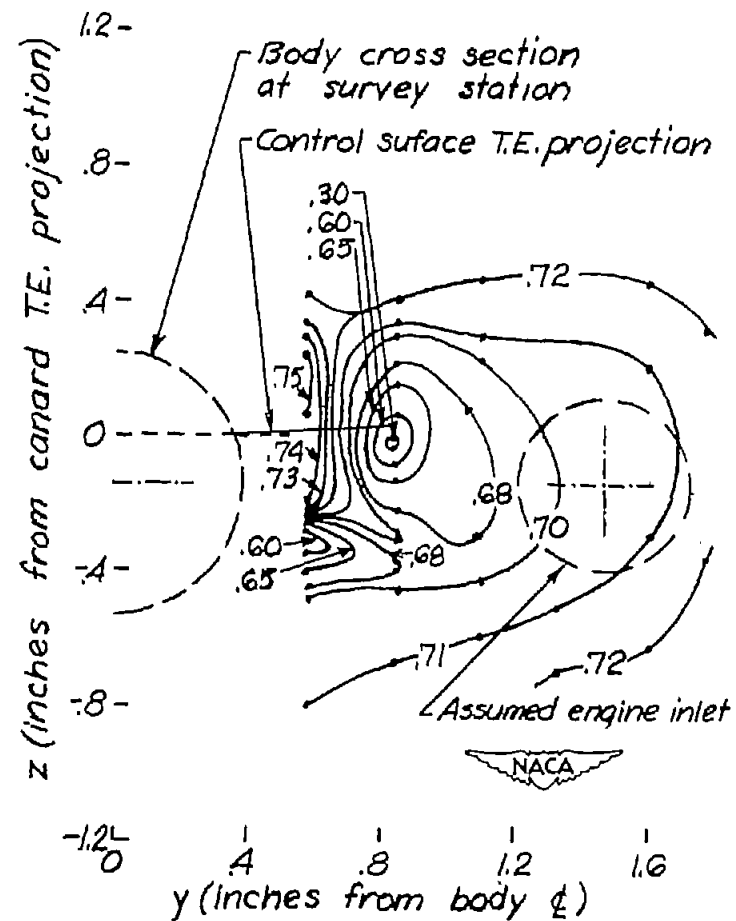


(d) $\alpha = 3.5^\circ$; $H_0 = 32.9$ in. Hg abs.

Figure 15.- Concluded.

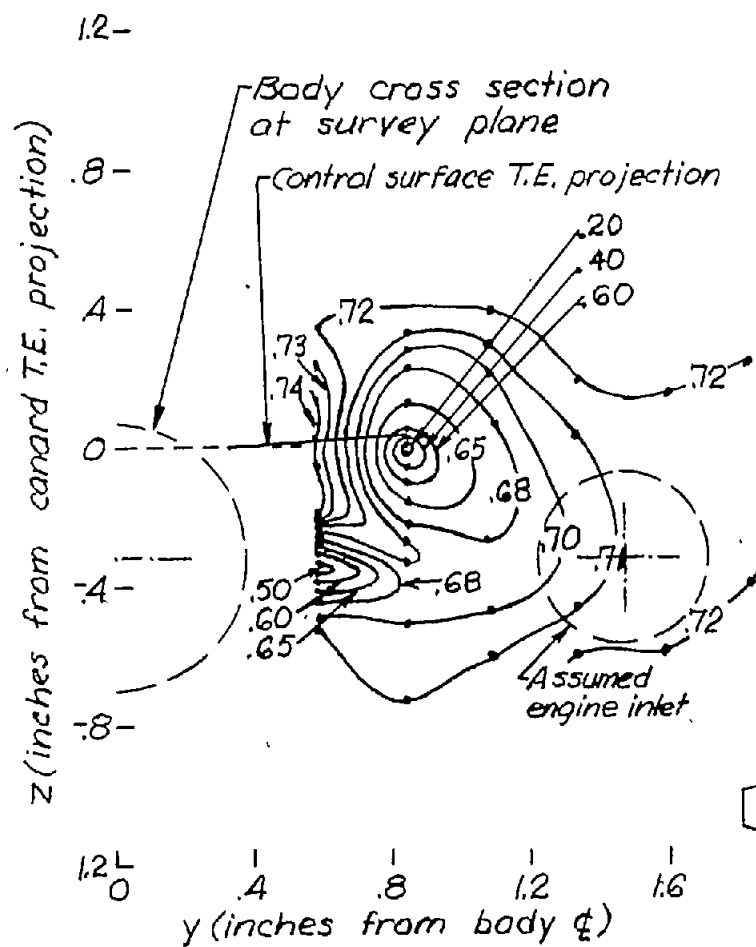


(a) $\alpha = 0^\circ$; $H_0 = 114.4$ in. Hg abs

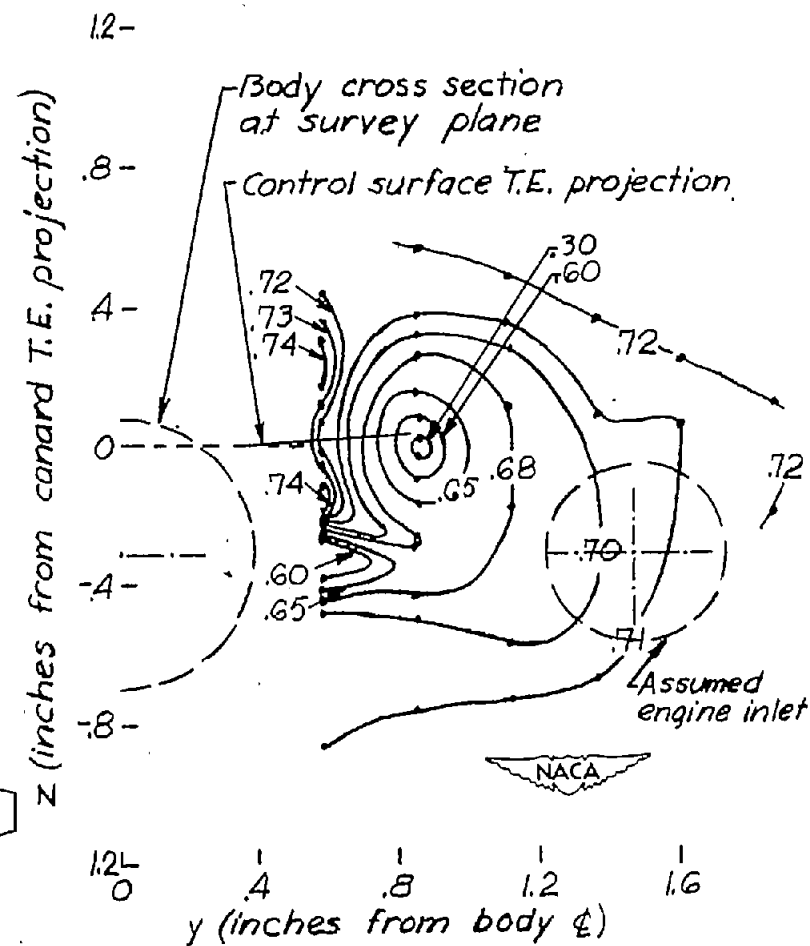


(b) $\alpha = 2^\circ$; $H_0 = 114.4$ in. Hg abs.

Figure 16.- Contours for the values of H_3/H_0 behind control surface 4B
(0.697 straight taper, 4-percent hexagonal section).

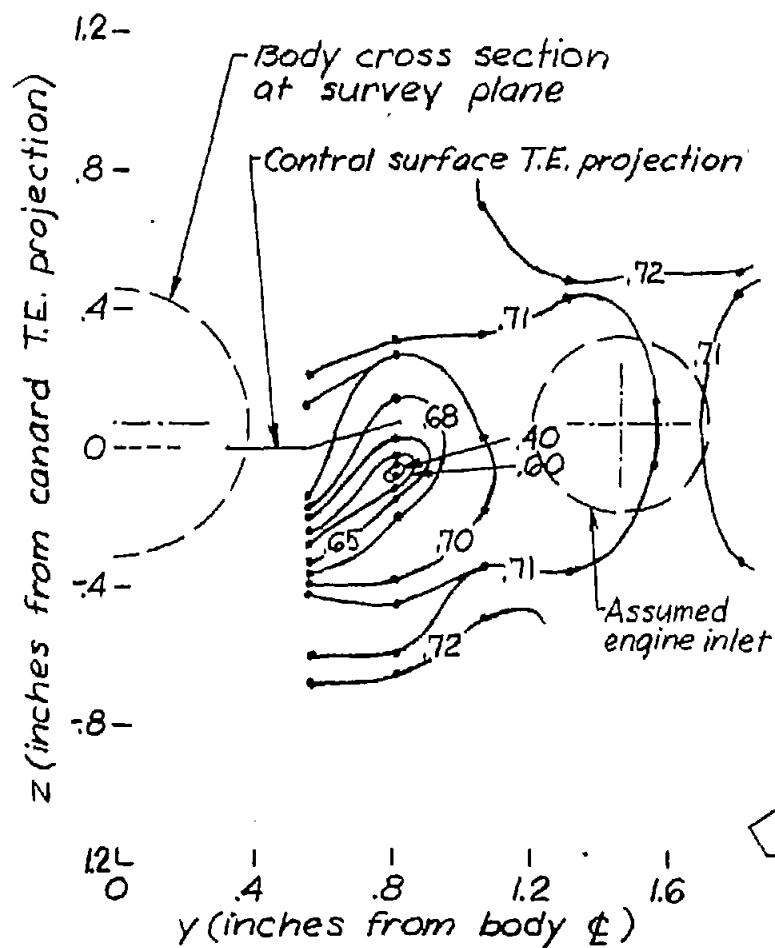


(c) $\alpha = 3.5^\circ$; $H_o = 31.3$ in. Hg abs.

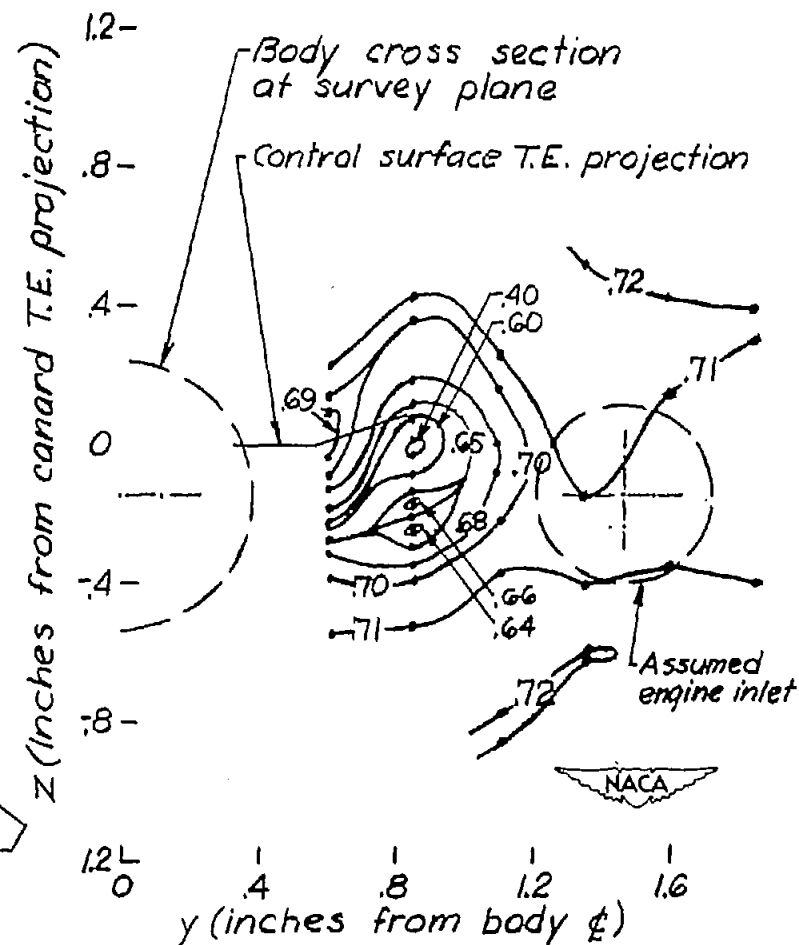


(d) $\alpha = 3.5^\circ$; $H_o = 114.1$ in. Hg abs.

Figure 16.- Concluded.

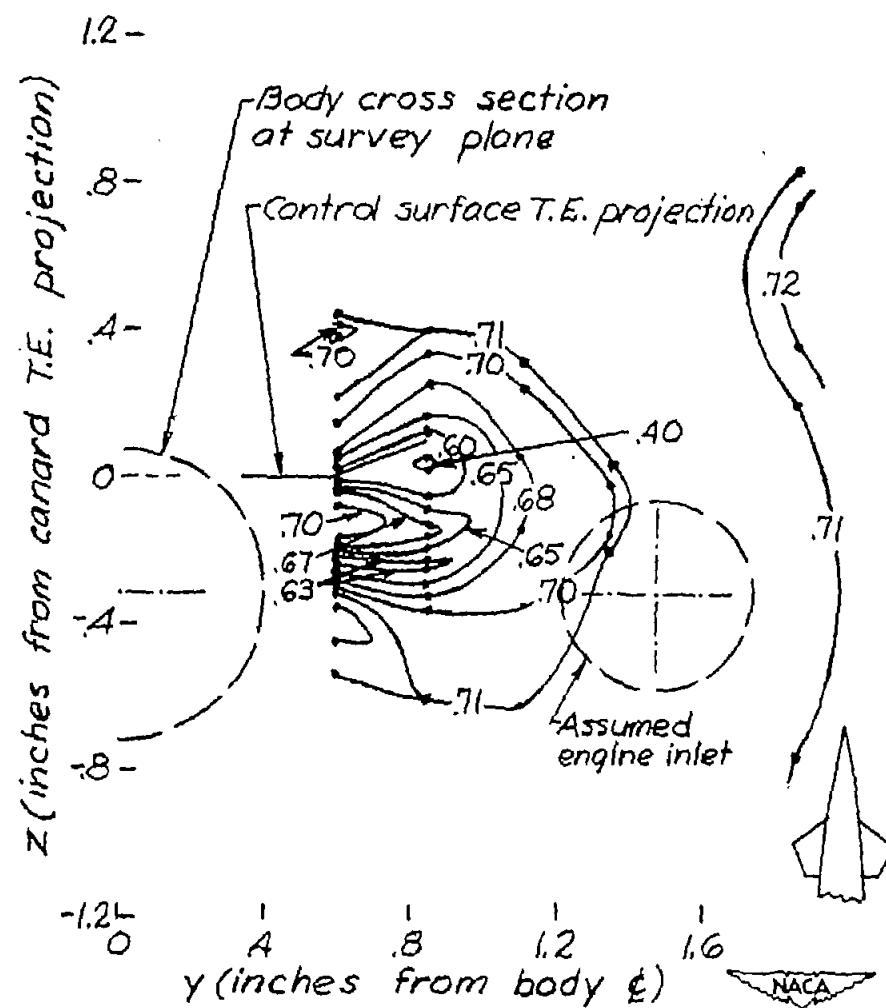


(a) $\alpha = 0^\circ$; $H_0 = 113.6 \text{ in. Hg abs.}$



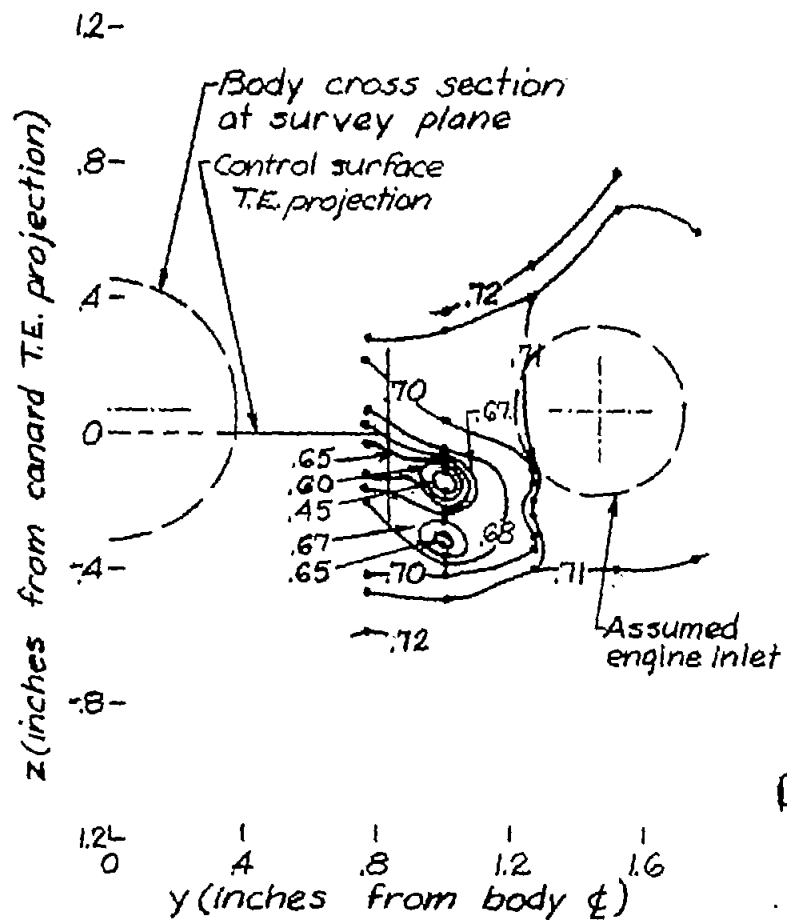
(b) $\alpha = 2^\circ$; $H_0 = 113.8 \text{ in. Hg abs.}$

Figure 17.- Contours for the values of H_3/H_0 behind control surface 1F (control surface 1A with tips raked 30°).

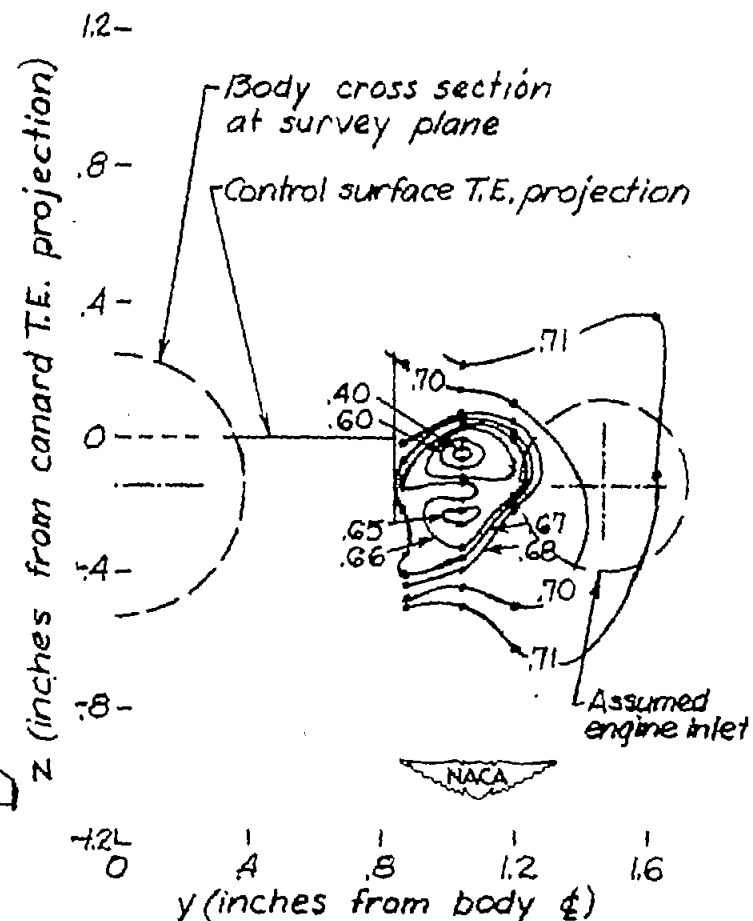


(c) $\alpha = 3.5$; $H_0 = 114.0$ in.Hg abs.

Figure 17.- Concluded.

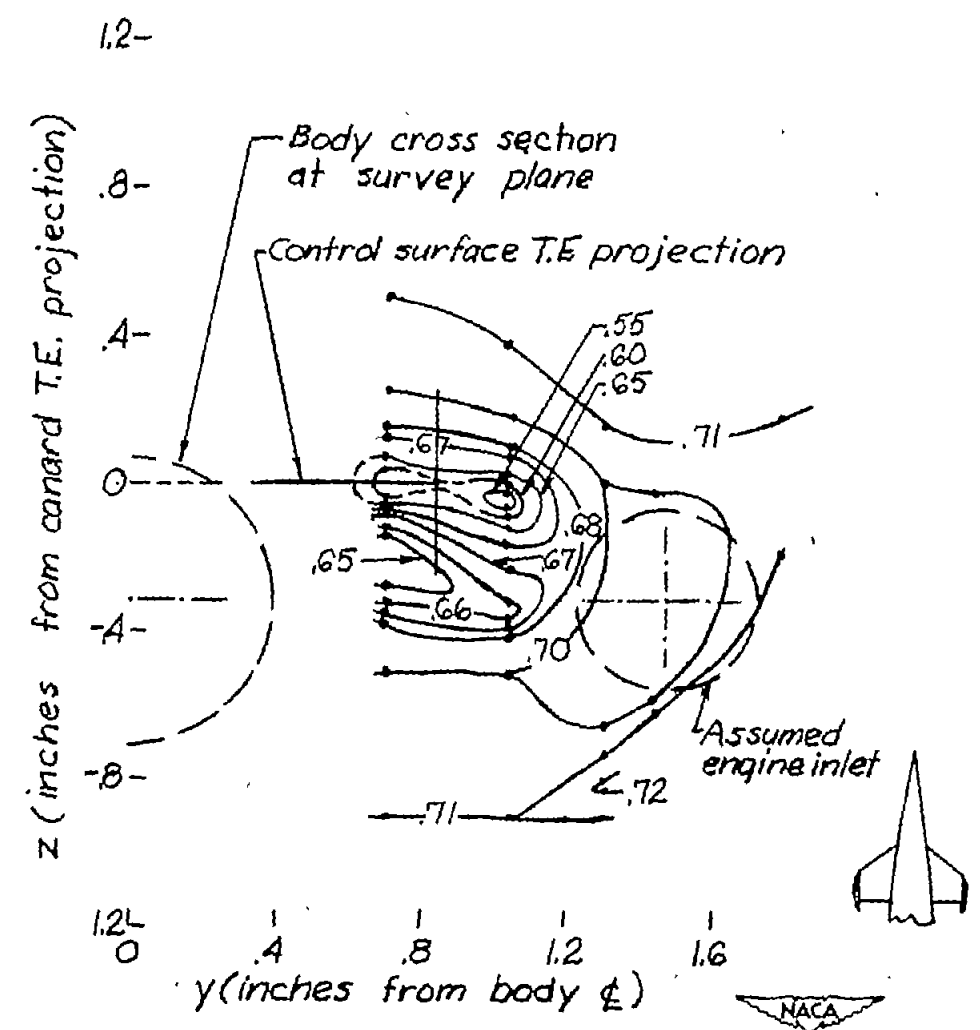


(a) $\alpha = 0^\circ$; $H_0 = 113.7$ in. Hg abs.



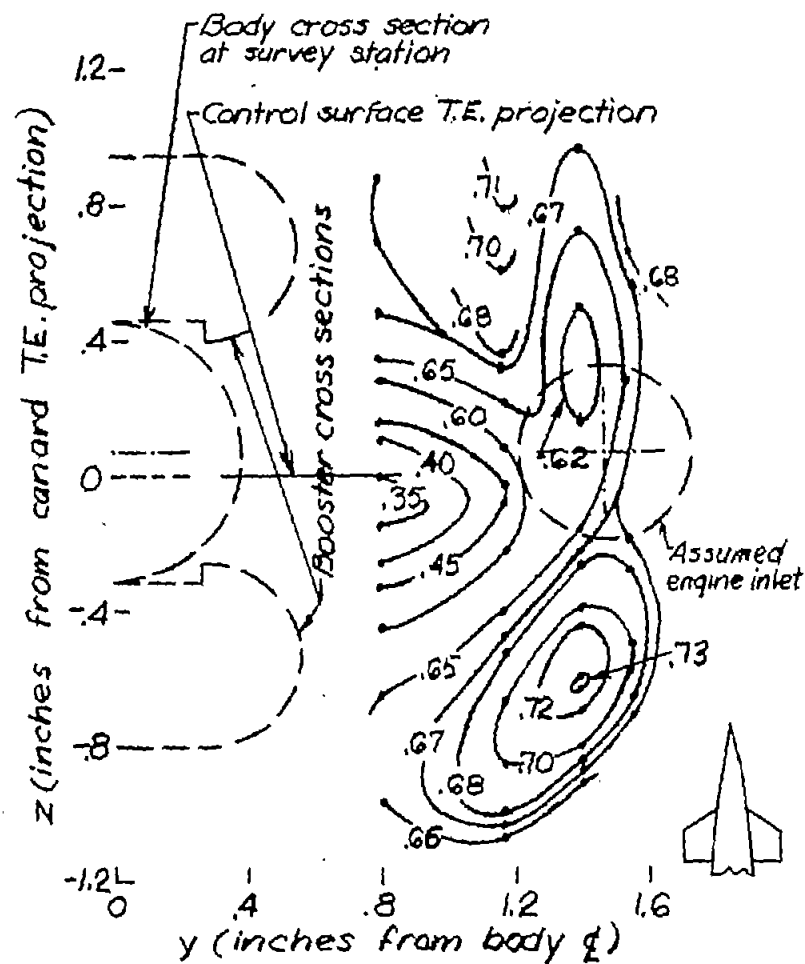
(b) $\alpha = 2^\circ$; $H_0 = 114.1$ in. Hg abs.

Figure 18.- Contours for the values of H_3/H_0 behind control surface 1E (control surface 1A with end plates).

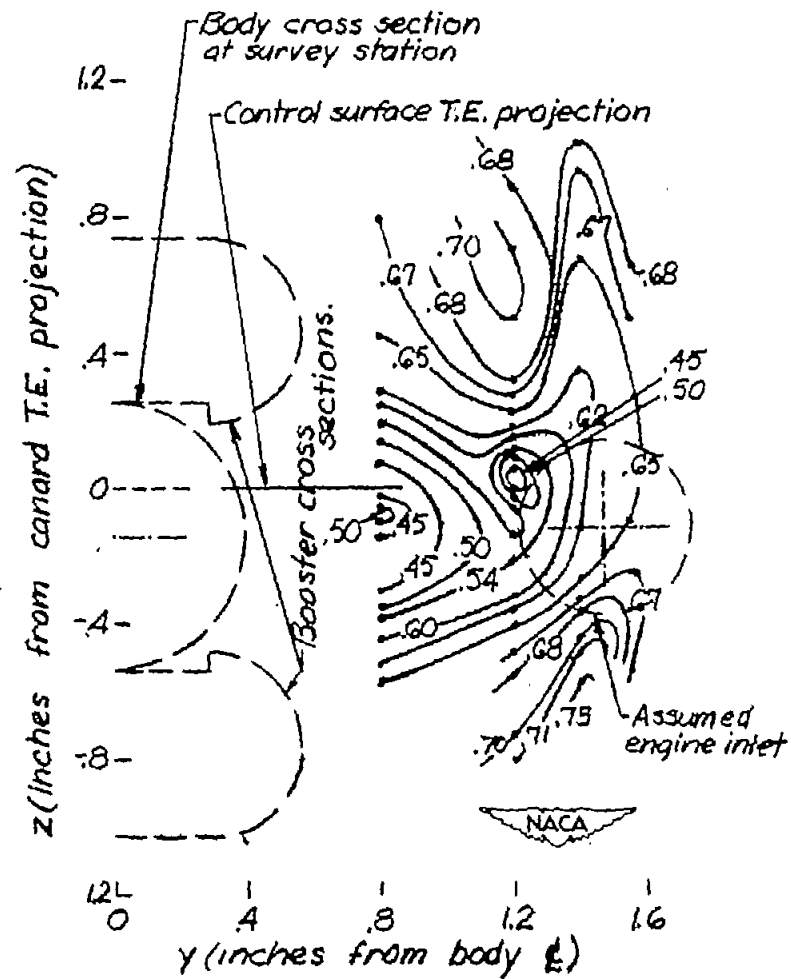


(c) $\alpha = 3.5^\circ$; $H_0 = 114.2$ in.Hg abs.

Figure 18.- Concluded.

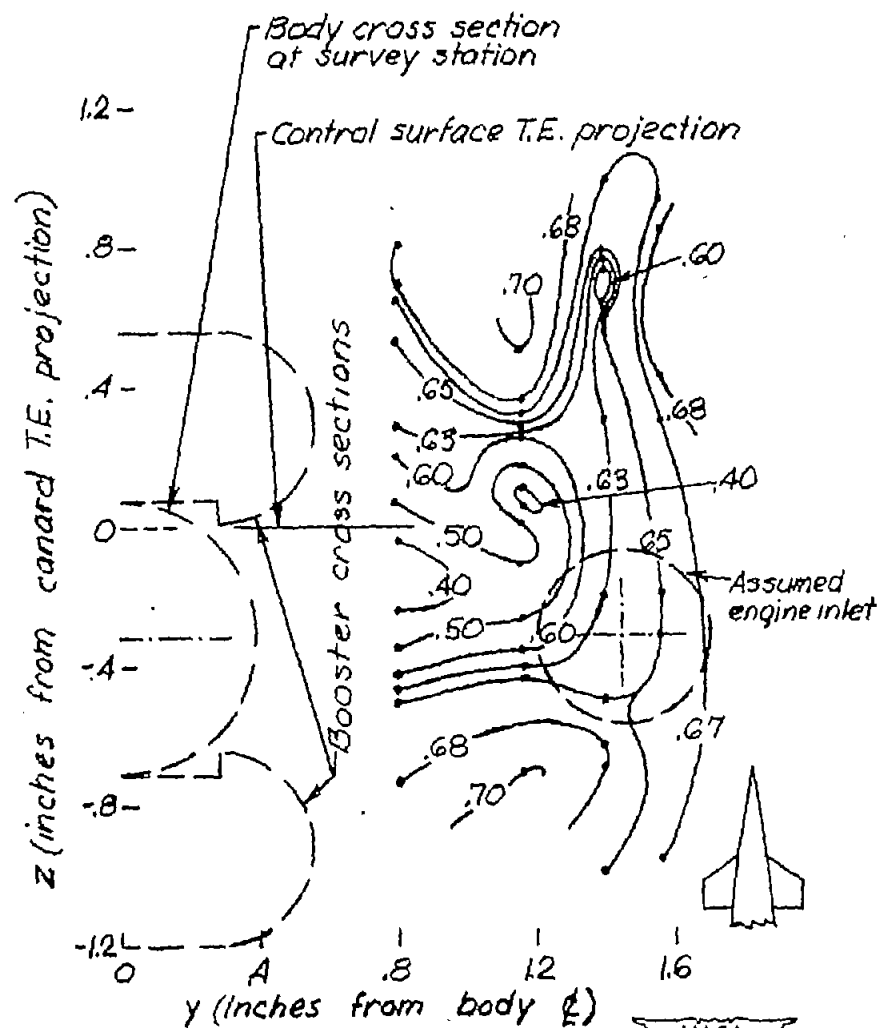


(a) $\alpha = 0^\circ$; $H_0 = 114.2$ in. Hg abs.



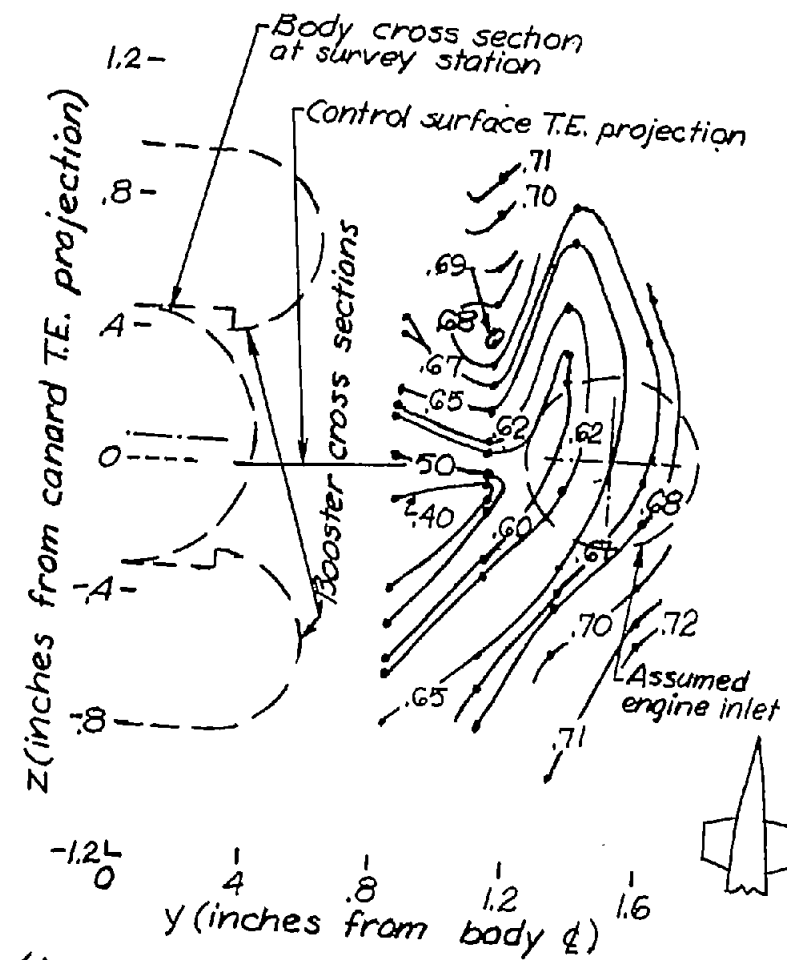
(b) $\alpha = 2^\circ$; $H_0 = 114.2$ in. Hg abs.

Figure 19.- Contours for the values of H_3/H_0 behind control surface 1D (control surface 1A with boosters on the body).

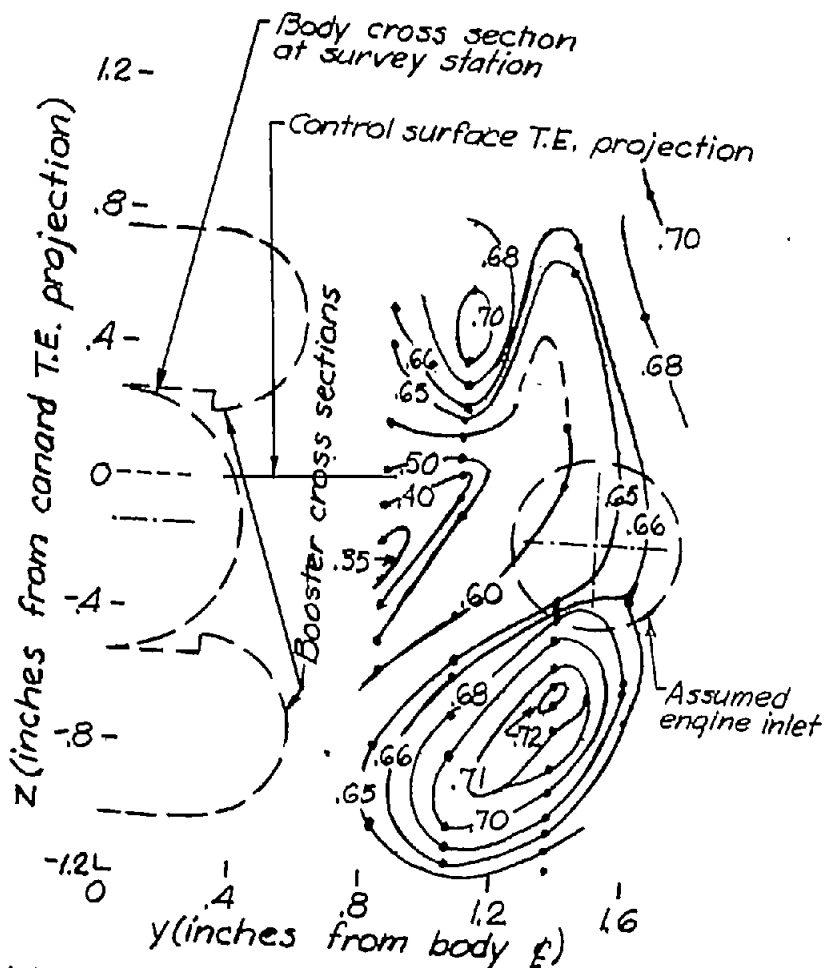


(c) $\alpha = 3.5^\circ$; $H_0 = 114.5$ in. Hg abs.

Figure 19.- Concluded.

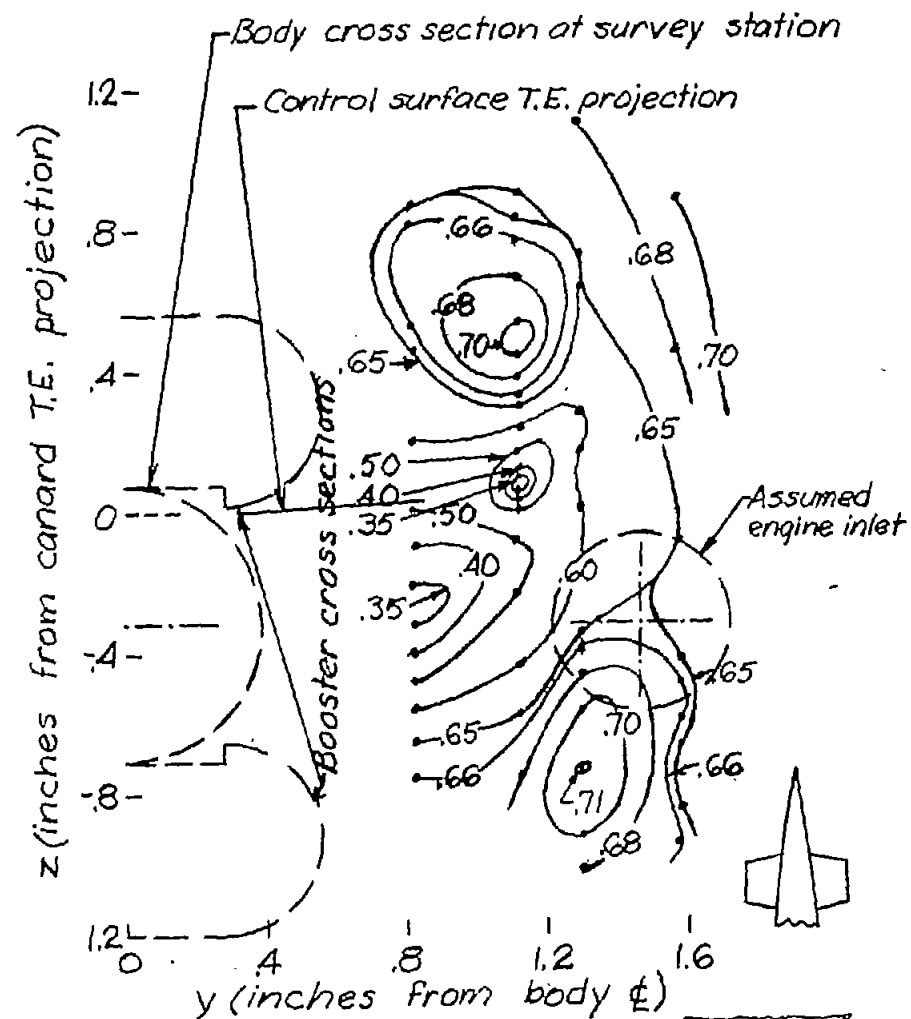


(a) $\alpha = 0^\circ$; $H_0 = 114.8$ in. Hg abs.



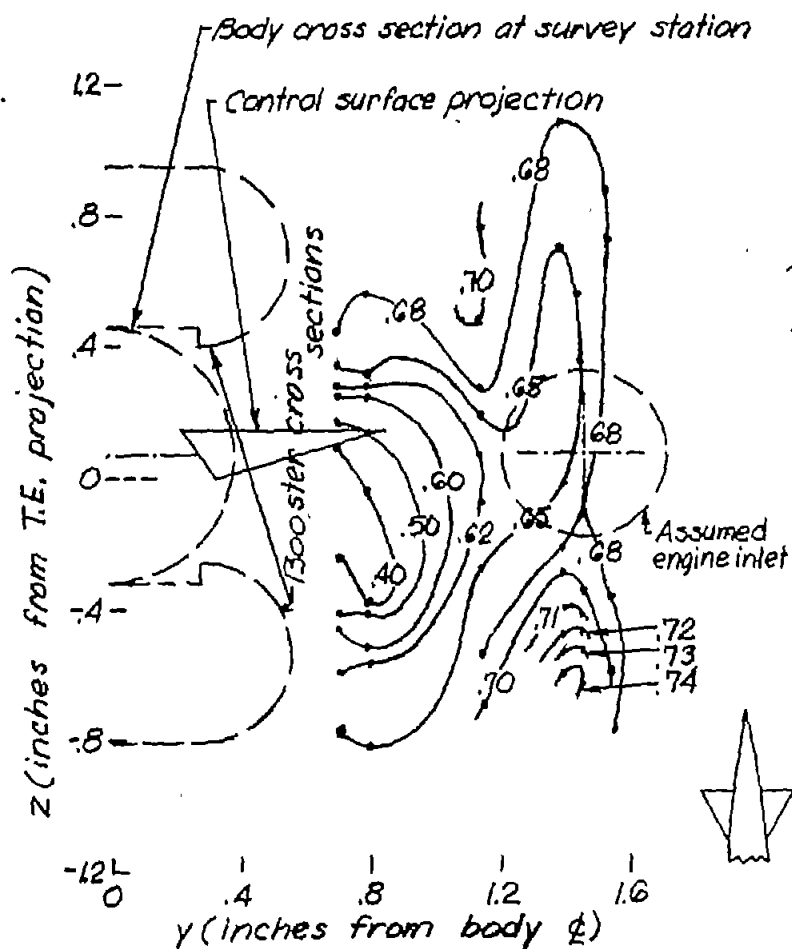
(b) $\alpha = 2^\circ$; $H_0 = 114.9$ in. Hg abs.

Figure 20.- Contours for the values of H_3/H_0 behind control surface 4C (control surface 4A with boosters on the body).

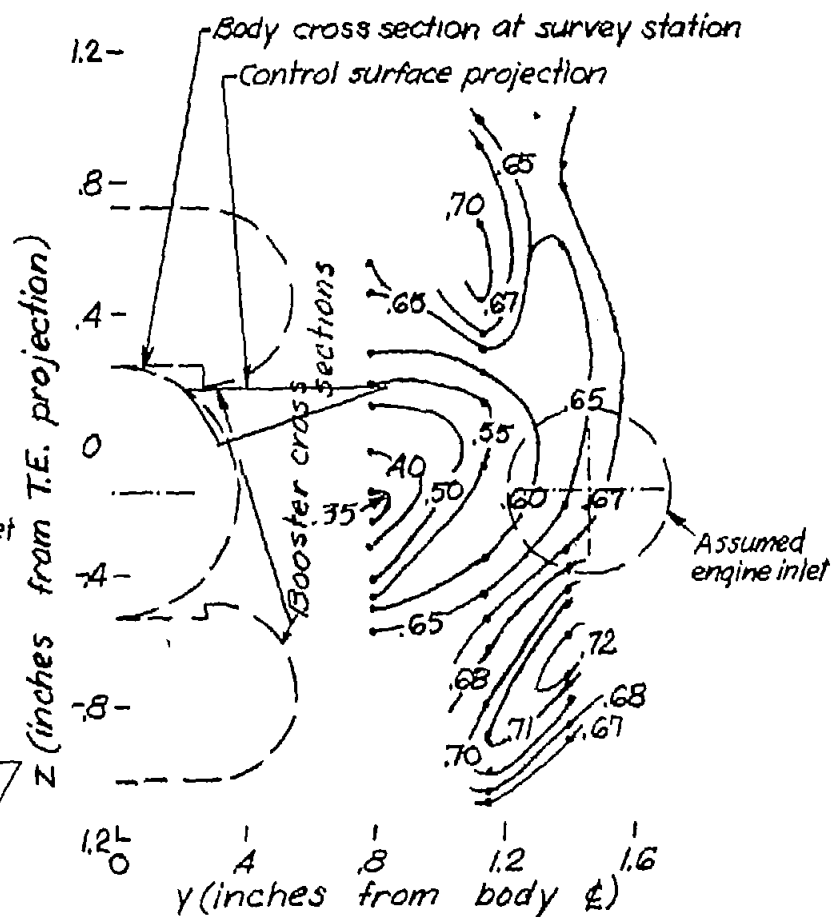


(c) $\alpha = 3.5^\circ$; $H_0 = 114.8$ in. Hg abs.

Figure 20.- Concluded.



(a) $\alpha = 0^\circ$; $H_0 = 114.4$ in. Hg abs.



(b) $\alpha = 2^\circ$; $H_0 = 114.3$ in. Hg abs.

Figure 21.- Contours for the values of H_3/H_0 behind control surface 2B
(control surface 2A with boosters on the body).

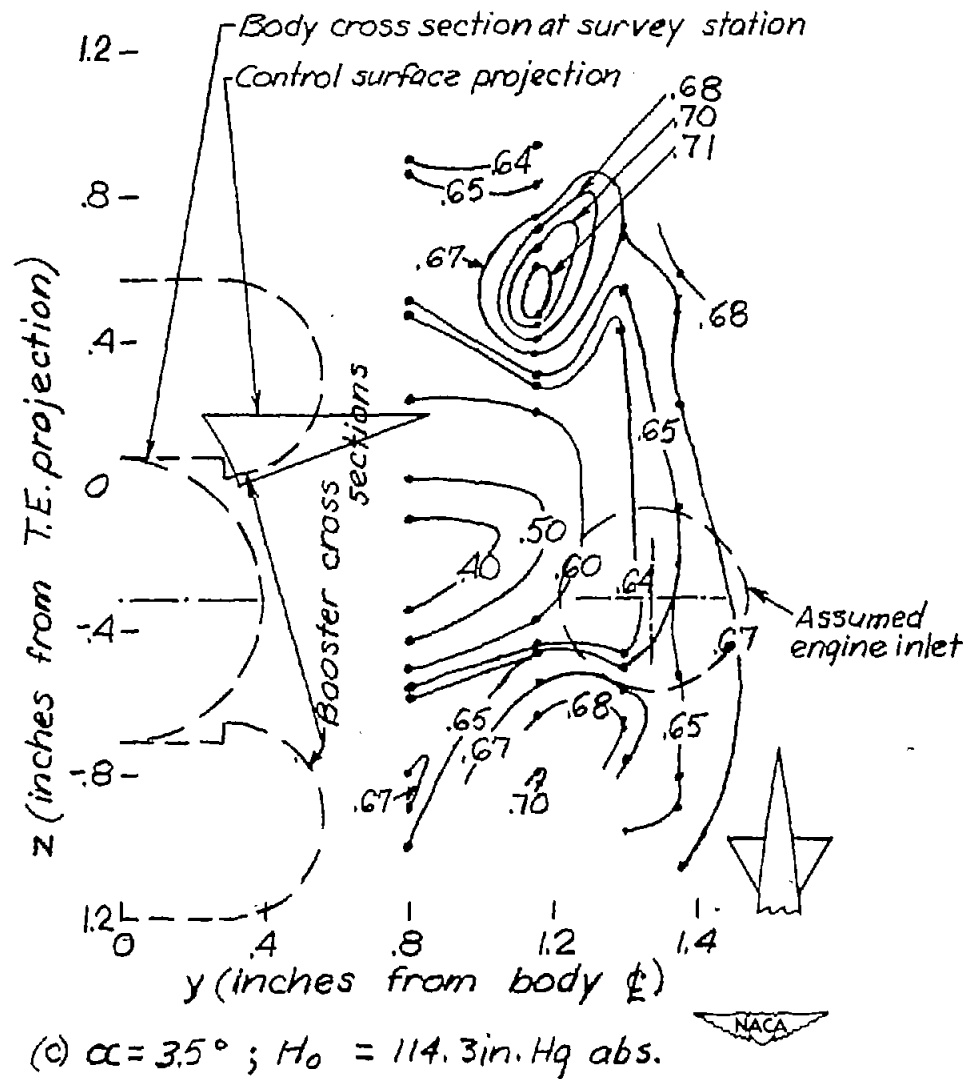


Figure 21.- Concluded.